SIAM J. APPL. MATH.
Vol. 84, No. 3, pp. 1227–1253

A STABILIZING EFFECT OF ADVECTION ON PLANAR INTERFACES IN SINGULARLY PERTURBED REACTION-DIFFUSION EQUATIONS*

PAUL CARTER†

Abstract. We consider planar traveling fronts between stable steady states in two-component singularly perturbed reaction-diffusion-advection equations, where a small quantity δ^2 represents the ratio of diffusion coefficients. The fronts under consideration are large amplitude and contain a sharp interface, induced by traversing a fast heteroclinic orbit in a suitable slow-fast framework. We explore the effect of advection on the spectral stability of the fronts to long wavelength perturbations in two spatial dimensions. We find that for suitably large advection coefficient ν, the fronts are stable to such perturbations, while they can be unstable for smaller values of ν. In this case, a critical asymptotic scaling $\nu \sim \delta^{-4/3}$ is obtained at which the onset of instability occurs. The results are applied to a family of traveling fronts in a dryland ecosystem model.

Key words. spectral stability, interfaces, reaction diffusion advection equations, geometric singular perturbation theory, ecosystem dynamics

MSC codes. 35K57, 35B25, 34D15, 35C07

DOI. 10.1137/23M1610872

1. Introduction.

We consider two-component reaction-diffusion-advection equations of the form

$$U_t = \Delta U + F(U,V;\boldsymbol{\mu}),$$
$$V_t = \frac{1}{\delta^2}\Delta V + G(U,V;\boldsymbol{\mu}) + \nu V_x, \qquad (1.1)$$

where $U(x,y,t), V(x,y,t) : \mathbb{R}^2 \times \mathbb{R} \to \mathbb{R}$, F, and G are smooth functions, and $\boldsymbol{\mu} \in \mathbb{R}^m$ denotes a collection of system parameters. We assume that (1.1) is singularly perturbed, with $0 < \delta \ll 1$. The advection coefficient $0 \le \nu < \infty$ is arbitrary. We consider planar interfaces between spatially homogeneous stable steady state solutions $(U,V)(x,y,t) = (U^\pm, V^\pm)$ of (1.1). The planar interfaces manifest as traveling wave solutions $(U,V)(x,y,t) = (u_\mathrm{h}, v_\mathrm{h})(\xi), \xi = x - ct$, which propagate with constant speed c in the x-direction, and are constant in the y-direction, and asymptotically approach the steady states $\lim_{\xi\to\pm\infty}(u_\mathrm{h}, v_\mathrm{h})(\xi) = (U^\pm, V^\pm)$.

Reaction-diffusion-advection systems arise in models of diverse phenomena such as pattern formation in mussel beds [7] and plankton [41], fog and wind induced vegetation alignment [9], disease spread [28], and population dynamics [15]. Here, we are primarily motivated by the phenomenon of desertification fronts in water-limited ecosystems [56], in which the bare-soil state slowly invades a vegetated state, resulting in (typically irreversible) desertification [30, 53], and similarly the reverse mechanism of vegetation fronts, in which vegetation invades a bare soil state. Instabilities in the resulting planar interface between vegetation and bare soil have been linked to spatial pattern formation [3, 14, 25]; see also section 6. Similar interfaces also appear

*Received by the editors October 23, 2023; accepted for publication (in revised form) March 21, 2024; published electronically June 10, 2024.
https://doi.org/10.1137/23M1610872
Funding: The author gratefully acknowledges support from the National Science Foundation through the grant DMS-2105816.
†Department of Mathematics, University of California, Irvine, Irvine, CA 92697 USA (pacarter@uci.edu).

in savanna/forest ecosystems, cloud formation, salt marshes, and other applications [6, 39].

Our aim is to examine the effect of the advection term νV_x on the stability of such an interface in two spatial dimensions. In systems of the form (1.1), the relation between diffusive and advective dynamics is known to impact the stability of planar stripes and periodic patterns [49, 50], and in particular, the presence of advection can have a stabilizing effect in the direction along the stripe [36]. We aim to explore the stabilizing effect of advection, focussing on long wavelength instabilities in the case of a single planar interface between stable steady states. We note that such interfaces in the class of equations (1.1) were previously studied in the absence of advection, i.e., $\nu = 0$, on infinite [14] and cylindrical domains [51, 52].

In the context of the motivating example of vegetation pattern formation in dryland ecosystem models, the quantities U and V represent interacting species and/or resources, for example U may represent vegetation biomass, and V represents water availability. In such models, it is natural to have widely separated diffusion coefficients due to the differing length and/or time scales on which water is transported and on which different vegetation species evolve [44]. In this setting, the advection term represents a slope in the topography, leading to downhill flow of water, and thus an anisotropy in the system. Observations suggest that the absence of advection (that is, flat terrain) lead to spotted and/or labrynthine patterns, whereas on sloped terrain vegetation may align in bands, consisting of interfaces alternating between vegetated and desert states [4, 16, 17, 27, 40, 54]. These interfaces align perpendicular to the slope, suggesting that the downhill flow of water prescribes a preferred orientation of the interface [42]. In [14] it was shown that such planar interfaces are unstable in many ecosystem models in the absence of advection, and it is the goal of this work to examine the effect of advection on the (in)stability of such interfaces. In particular, we demonstrate that sufficiently large advection has a stabilizing effect on interfaces in two spatial dimensions, with respect to long wavelength perturbations in the y-direction, transverse to the direction of propagation.

In the spirit of [14], our results are framed in the context of a geometric singular perturbation analysis of the traveling wave equation associated with (1.1), under suitable assumptions about the underlying geometry of the system. The novel contribution of the current study is the inclusion of the advection term; the coefficient ν can be small or large relative to the small parameter δ, naturally leading to a three timescale system. Systems with more than two timescales, and potentially multiple interacting singular limits, are responsible for complex dynamics in many applications [13, 18, 33, 37] and present challenges in the direct use of geometric singular perturbation methods, which are typically formulated for two-timescale systems. However, for systems with multiple small (or large) parameters, geometric singular perturbation methods can be used to identify critical overlapping scaling regimes, analyze the system separately in each regime, and piece the analyses together to obtain a complete picture of the dynamics in the presence of multiple singular limits [37]. In particular, in the system (1.1), using a formal asymptotic approach inspired by geometric singular perturbation methods, we are able to obtain a simple explicit criterion for (in)stability of planar interfaces, depending on the relative scaling of ν, δ, and we identify a potential onset of (in)stability at a critical scaling $\nu \sim \delta^{-4/3}$. The results can be easily applied to fronts in reaction-diffusion-advection models, and we demonstrate the applicability of the results to a dryland ecosystem model in section 5.

We note that the results also apply to systems of the form

$$\begin{aligned} U_t &= \Delta U + F(U,V;\boldsymbol{\mu}) + \nu_1 U_x,\\ V_t &= \frac{1}{\delta^2}\Delta V + G(U,V;\boldsymbol{\mu}) + \nu_2 V_x \end{aligned} \tag{1.2}$$

for arbitrary advection coefficients $\nu_i \in \mathbb{R}$. By shifting to a traveling coordinate frame, and reversing the spatial variable x if necessary, this system can be transformed to (1.1), defining $0 \le \nu = |\nu_1 - \nu_2| < \infty$ as the differential flow [45, 49]. Additionally, we note that the reaction terms F and G in (1.1) do not depend explicitly on δ or ν. While one could consider such a dependence in a given model with explicit reaction terms, we will see that the behavior of this system depends critically on certain relative scalings between the parameters δ and ν. To avoid additionally tracking these scalings within the reaction terms themselves throughout the various scaling regimes, for simplicity we assume they are independent of (δ,ν).

2. Setup.

2.1. Traveling wave formulation. To capture traveling front solutions which propagate in the direction determined by the advection term, we move into a traveling coordinate frame $\xi = x - ct$ and obtain the system

$$\begin{aligned} U_t &= U_{\xi\xi} + U_{yy} + cU_\xi + F(U,V),\\ V_t &= \frac{1}{\delta^2}(V_{\xi\xi} + V_{yy}) + (\nu + c)\,V_\xi + G(U,V), \end{aligned} \tag{2.1}$$

where we drop the explicit dependence on the system parameters $\boldsymbol{\mu}$. We search for stationary solutions $(U,V)(\xi,y,t) = (u,v)(\xi)$, which are constant in the y-direction, and thus propagate with constant speed c in the x-direction. This results in the traveling wave ODE

$$\begin{aligned} 0 &= u_{\xi\xi} + cu_\xi + F(u,v),\\ 0 &= v_{\xi\xi} + \delta^2(\nu + c)v_\xi + \delta^2 G(u,v). \end{aligned} \tag{2.2}$$

The system (2.2) can then be written as the first order system

$$\begin{aligned} u_\xi &= p,\\ p_\xi &= -cp - F(u,v),\\ v_\xi &= \delta q,\\ q_\xi &= -\delta^2(\nu + c)q - \delta G(u,v), \end{aligned} \tag{2.3}$$

where the homogeneous rest states $(U^\pm, V^\pm)$ of (1.1) correspond to fixed points $P^\pm = (U^\pm, 0, V^\pm, 0)$ of (2.3), and traveling fronts between the rest states $(U^\pm, V^\pm)$ correspond to heteroclinic orbits between the fixed points $P^\pm$ in (2.3).

To analyze traveling front solutions in (2.2), we use geometric singular perturbation theory [24]. Throughout, we assume that $\delta \ll 1$ is a small parameter, but the parameter ν can be small or large. Thus in the regime $\delta \ll 1$, this system can have up to three timescales, determined by the relation between the two parameters ν, δ, and we must therefore separate the analysis of (2.2) into cases, depending on the relative size of the parameters ν, δ.

The following singular perturbation analysis distinguishes between three cases, depending on which parameter is used as the primary singular perturbation parameter, and we describe the slow-fast structure of traveling fronts in each of these regions

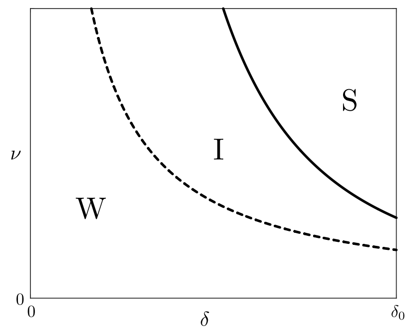

FIG. 1. *Shown is a schematic of the different scaling regimes considered. The dashed and solid curves represent the boundary curves* $\nu = \frac{\bar{R}_0}{\delta}$ *and* $\nu = \frac{r_0}{\delta^2}$*, respectively, as described in section* 2.3. *The weak advection (W), intermediate (I), and strong advection (S) regimes are labeled accordingly.*

for sufficiently small $0 < \delta \ll 1$. In the weak advection regime $0 \leq \nu \leq \mathcal{O}(\delta^{-1})$, δ serves as the timescale separation parameter, while in the strong advection regime $\nu \geq \mathcal{O}(\delta^{-2})$, the quantity $\varepsilon := \nu^{-1} \ll 1$ is taken as the timescale separation parameter. In the intermediate regime $\mathcal{O}(\delta^{-1}) \leq \nu \leq \mathcal{O}(\delta^{-2})$, the advection-diffusion coefficient "ratio" $r := \delta^2\nu$ is taken as the primary singular perturbation parameter. By combining the results in these regions, we are able to describe the slow-fast structure of traveling front solutions for each (ν, δ) satisfying $\nu \geq 0, 0 < \delta \leq \delta_0$ for some $\delta_0 > 0$; see Figure 1 and section 2.3. Due to the appearance of the $\delta^2\nu$ coefficient in (2.2), the quantity r will, in fact, play an important role throughout the three regimes.

In each regime, the set $\mathcal{S} = \{F(u,v) = 0\}$ organizes the dynamics, as this set helps define the critical manifold(s) which appear in the slow-fast formulation of the traveling wave problem. Generically, on a given compact set, away from points where $F_u = 0$, $\mathcal{S}$ is formed by the union of a finite number of branches $\mathcal{S}_j$, $j = 1, \ldots, N$, which can be written as graphs $u = f_j(v)$ satisfying $F(f_j(v), v) = 0$ for $v \in I_j$, where I_j is an interval. Among these, we identify those branches which contain the steady states $(U^\pm, V^\pm)$; in particular, we denote by $f^\pm$ the functions, defined on intervals $v \in I_v^\pm$, which define the graphs corresponding to the two branches $\mathcal{S}^\pm$ of $\mathcal{S}$ satisfying $f^\pm(V^\pm) = U^\pm$, and we let $F_u^\pm$ denote $\frac{\partial F}{\partial u}(U^\pm, V^\pm)$, etc. Independent of the specific parameter regime, we make the following basic assumptions regarding the steady states $(U^\pm, V^\pm)$.

Assumption 1 (steady states).

(i) There exist two homogeneous steady states $(U^\pm, V^\pm)$ which are stable as solutions of (1.1) for $0 < \delta \ll 1$ and all $\nu \geq 0$. In particular, we assume (see Appendix A)

$$F_u^\pm < 0, \qquad G_v^\pm < 0, \qquad F_u^\pm G_v^\pm - F_v^\pm G_u^\pm > 0. \tag{2.4}$$

(ii) The states $(U^\pm, V^\pm)$ lie on different branches of $\mathcal{S}$, that is, $f^-(v) \not\equiv f^+(v)$.

We will analyze traveling front solutions $(u,v)(\xi)$ satisfying $\lim_{\xi\to\pm\infty}(u,v)(\xi) = (U^\pm, V^\pm)$; see Figure 2. The first condition (i) ensures that such a front is *bistable,* so that it forms an interface between asymptotically stable rest states; we will see that the resulting conditions (2.4) ensure hyperbolicity of relevant critical manifolds and the rest states in their associated reduced flows. We also remark that the condition on $G_v^\pm$ ensures the steady states remain stable for large advection $\nu \gg 1$ (see Appendix A);

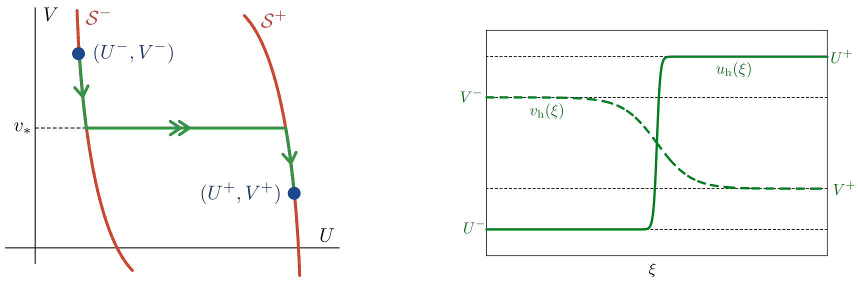

FIG. 2. *(Left) The steady states $(U^{\pm}, V^{\pm})$ and the branches $\mathcal{S}^{\pm}$ of the nullcline $F(U,V) = 0$. (Right) Schematic of a traveling front solution $(u_{\mathrm{h}}, v_{\mathrm{h}})(\xi)$ with a single sharp interface.*

this prevents instabilities which can arise in the background states $(U^{\pm}, V^{\pm})$ due to large differential flow [8, 45, 49], so that we focus only on instabilities which arise due to the interface itself.

The second condition (ii) ensures that the front interface is sharp; that is, in the appropriate slow-fast formulation (depending on the specific asymptotic regime of the parameters δ, ν), the front (in an appropriate singular limit) must traverse a singular fast heteroclinic orbit $u_*(\xi)$ of an associated layer problem in the subspace $v = v_*$ with leading order speed $c = c_*$, as opposed to being entirely contained within the reduced flow on a single connected branch of a slow manifold; for the latter situation; see, e.g., [19]. The solution $u_*(\xi)$ solves the simpler scalar traveling wave equation

$$0 = u_{\xi\xi} + c_* u_\xi + F(u, v_*), \tag{2.5}$$

and forms a fast connection between the branches of $\mathcal{S}$, that is, $u_*^{\pm} := \lim_{\xi\to\pm\infty} u_*(\xi)$ satisfy $u_*^{\pm} = f^{\pm}(v_*)$. The existence of such a heteroclinic orbit in (2.5) can, for instance, be obtained in a given system using phase plane techniques. The fronts under consideration here traverse only one such fast heteroclinic orbit, i.e., they do not jump back and forth between several branches of $\mathcal{S}$.

Beyond the conditions (i)–(ii) on the steady states $(U^{\pm}, V^{\pm})$, additional structure is required concerning the reduced flows of certain critical manifolds which appear in the existence problem to allow for bistable traveling front solutions between $(U^{\pm}, V^{\pm})$. However, since these conditions are related to the specific slow-fast formulation in each parameter regime, we delay their discussion until introducing the slow-fast structure of the fronts; see Assumptions 4 and 5 in sections 3 and 4, respectively. In the following section, we focus on the stability criterion which arises given a traveling wave solution which connects the steady states $(U^{\pm}, V^{\pm})$.

2.2. Long-wave (in)stability of planar interfaces. Given a traveling wave solution $\phi_{\mathrm{h}}(\xi; r, \delta) = (u_{\mathrm{h}}, v_{\mathrm{h}})(\xi; \nu, \delta)$ of (2.1) with speed $c = c(\nu, \delta)$ satisfying $\lim_{\xi\to\pm\infty} \phi_{\mathrm{h}}(\xi; \nu, \delta) = (U^{\pm}, V^{\pm})$, we linearize (2.1) using the ansatz $(U, V)(\xi, y, t) = (u_{\mathrm{h}}, v_{\mathrm{h}})(\xi; \nu, \delta) + (u, v)(\xi) e^{\lambda t + i\ell y}$, which results in the corresponding linear stability problem

$$\begin{aligned} \lambda u &= u_{\xi\xi} + c u_\xi - \ell^2 u + F_u(u_{\mathrm{h}}(\xi), v_{\mathrm{h}}(\xi)) u + F_v(u_{\mathrm{h}}(\xi), v_{\mathrm{h}}(\xi)) v, \\ \lambda v &= \frac{1}{\delta^2} v_{\xi\xi} + (\nu + c)\, v_\xi - \frac{\ell^2}{\delta^2} v + G_u(u_{\mathrm{h}}(\xi), v_{\mathrm{h}}(\xi)) u + G_v(u_{\mathrm{h}}(\xi), v_{\mathrm{h}}(\xi)) v, \end{aligned} \tag{2.6}$$

parameterized by the transverse Fourier wavenumber $\ell \in \mathbb{R}$. This can, equivalently, be written as the eigenvalue problem

$$\mathcal{L}\begin{pmatrix} u \\ v \end{pmatrix} = \lambda \begin{pmatrix} u \\ v \end{pmatrix} + \ell^2 \begin{pmatrix} u \\ \frac{1}{\delta^2} v \end{pmatrix}. \tag{2.7}$$

where

$$\mathcal{L} = \begin{pmatrix} \partial_{\xi\xi} + c\partial_\xi + F_u(u_\mathrm{h}(\xi), v_\mathrm{h}(\xi)) & F_v(u_\mathrm{h}(\xi), v_\mathrm{h}(\xi)) \\ G_u(u_\mathrm{h}(\xi), v_\mathrm{h}(\xi)) & \dfrac{1}{\delta^2}\partial_{\xi\xi} + (\nu + c)\,\partial_\xi + G_v(u_\mathrm{h}(\xi), v_\mathrm{h}(\xi)) \end{pmatrix}. \tag{2.8}$$

When $\ell = 0$, this eigenvalue problem is solved by taking $\lambda = 0$ and $(u, v) = (u_\mathrm{h}', v_\mathrm{h}')$ (due to translation invariance of the traveling wave ODE (2.2)). We make the following assumption regarding the stability of the front as a traveling wave in one space dimension, i.e., in the direction of propagation.

Assumption 2 (one-dimensional (1D) stability of the front). The operator $\mathcal{L}$ satisfies $\mathrm{spec}\{\mathcal{L}\} \subset \{\lambda \in \mathbb{C} : \mathrm{Re}\,\lambda < 0\} \cup \{0\}$. Furthermore, the eigenvalue $\lambda = 0$ is isolated and algebraically simple, and $\mathcal{L}$ has 1D generalized kernel spanned by the eigenfunction $(u_\mathrm{h}', v_\mathrm{h}')$.

In a given system, this assumption regarding 1D stability may be nontrivial to verify, and typically involves detailed estimates on the solution $(u_\mathrm{h}, v_\mathrm{h})(\xi; \nu, \delta)$ and careful analysis of (2.6) for $\ell = 0$ and λ in various regions of the complex plane. As this study is focused specifically on instabilities arising from the resulting *two-dimensional* (2D) interface, we do not pursue a detailed analysis of 1D stability here, but we note that this assumption can be verified for traveling fronts in specific systems using techniques of geometric singular perturbation theory, Lin's method, and/or Evans function approaches [5, 20, 43].

To study the stability of the front to long wavelength perturbations in two spatial dimensions, we examine how this eigenvalue problem perturbs for values of $|\ell| \ll 1$. Following the (formal) analysis of [14] for the stability problem (2.6), we expand the critical translation eigenvalue $\lambda_\mathrm{c}(\ell)$ satisfying $\lambda_\mathrm{c}(0) = 0$ and the corresponding eigenfunction $(u_\mathrm{c}, v_\mathrm{c})(\xi; \ell)$ as

$$\lambda_\mathrm{c}(\ell) = \lambda_{\mathrm{c},2}\ell^2 + \mathcal{O}(\ell^4), \qquad \begin{pmatrix} u_\mathrm{c}(\xi;\ell) \\ v_\mathrm{c}(\xi;\ell) \end{pmatrix} = \begin{pmatrix} u_\mathrm{h}'(\xi) \\ v_\mathrm{h}'(\xi) \end{pmatrix} + \ell^2 \begin{pmatrix} u_{\mathrm{c},2}(\xi) \\ v_{\mathrm{c},2}(\xi) \end{pmatrix} + \mathcal{O}(\ell^4). \tag{2.9}$$

Substituting into (2.7), at $\mathcal{O}(\ell^2)$, we have

$$\mathcal{L}\begin{pmatrix} u_{\mathrm{c},2} \\ v_{\mathrm{c},2} \end{pmatrix} = \lambda_{\mathrm{c},2} \begin{pmatrix} u_\mathrm{h}' \\ v_\mathrm{h}' \end{pmatrix} + \begin{pmatrix} u_\mathrm{h}' \\ \frac{1}{\delta^2} v_\mathrm{h}' \end{pmatrix}. \tag{2.10}$$

In order for this equation to admit a solution, the inhomogeneous term on the right-hand side must satisfy a Fredholm solvability condition [34]

$$\left\langle \lambda_{\mathrm{c},2} \begin{pmatrix} u_\mathrm{h}' \\ v_\mathrm{h}' \end{pmatrix} + \begin{pmatrix} u_\mathrm{h}' \\ \frac{1}{\delta^2} v_\mathrm{h}' \end{pmatrix}, \begin{pmatrix} u^A \\ v^A \end{pmatrix} \right\rangle_{L^2} = 0, \tag{2.11}$$

where $(u^A, v^A)(\xi)$ is the unique (up to scalar multiple) integrable eigenfunction of the corresponding adjoint equation

$$\mathcal{L}^A \begin{pmatrix} u \\ v \end{pmatrix} = 0, \tag{2.12}$$

where the adjoint operator $\mathcal{L}^A$ is given by

$$\mathcal{L}^A = \begin{pmatrix} \partial_{\xi\xi} - c\partial_\xi + F_u(u_\mathrm{h}(\xi), v_\mathrm{h}(\xi)) & G_u(u_\mathrm{h}(\xi), v_\mathrm{h}(\xi)) \\ F_v(u_\mathrm{h}(\xi), v_\mathrm{h}(\xi)) & \dfrac{1}{\delta^2}\partial_{\xi\xi} - (\nu + c)\,\partial_\xi + G_v(u_\mathrm{h}(\xi), v_\mathrm{h}(\xi)) \end{pmatrix}. \tag{2.13}$$

Equivalently, solving (2.11) for $\lambda_{\mathrm{c},2}$, we obtain

$$\lambda_{\mathrm{c},2} = -\frac{\int_{-\infty}^{\infty}\left(u_{\mathrm{h}}'(\xi)u^A(\xi) + \frac{1}{\delta^2}v_{\mathrm{h}}'(\xi)v^A(\xi)\right)\mathrm{d}\xi}{\int_{-\infty}^{\infty}\left(u_{\mathrm{h}}'(\xi)u^A(\xi) + v_{\mathrm{h}}'(\xi)v^A(\xi)\right)\mathrm{d}\xi}. \tag{2.14}$$

The sign of $\lambda_{\mathrm{c},2}$ determines the 2D stability of the front $(u_{\mathrm{h}}, v_{\mathrm{h}})$ to perturbations with small transverse wavenumber $|\ell| \ll 1$. As with the slow-fast structure of the fronts themselves, the structure of the stability problem (2.6) and the computation of the adjoint solution $(u^A, v^A)(\xi)$ change depending on the relative size(s) of the parameters ν, δ. Hence we must split the computation of $\lambda_{\mathrm{c},2}$ into cases corresponding to different scaling regimes as described in section 2.1.

2.3. Summary of results. By considering the slow-fast construction of traveling fronts in the weak advection, intermediate, and strong advection regimes, we determine leading order asymptotics for the critical coefficient $\lambda_{\mathrm{c},2}$ (2.14) which determines long wavelength instabilities along the front interface. We will see that the sign of this coefficient depends only on information encoded in the fast layer orbit $u_*(\xi)$ of (2.5) in the subspace $v = v_*$ in the singular slow-fast framework. We impose one additional nondegeneracy assumption

Assumption 3 (nondegeneracy condition). The quantity $G(u_*^+, v_*) - G(u_*^-, v_*) \neq 0$.

Under Assumptions 1–3, for a traveling front ϕ_{h} which traverses a single fast jump $u_*(\xi)$ of the reduced equation (2.5), we obtain an asymptotic long-wavelength stability criterion which holds throughout the weak advection, strong advection, and intermediate regimes. To summarize, letting r_0 and $\bar{R}_0$ denote sufficiently small and sufficiently large fixed positive constants, respectively, for sufficiently small $\delta_0 > 0$ we find the following asymptotic stability criteria by determining the sign of $\lambda_{\mathrm{c},2}$ for $0 < \delta \ll \delta_0 \ll 1$:

- **Weak advection regime:** $0 \leq \nu \leq \frac{\bar{R}_0}{\delta}$. In this regime, to leading order

  $$\mathrm{sign}(\lambda_{\mathrm{c},2}) = -\mathrm{sign}(F_*) \times \mathrm{sign}(G_*), \tag{2.15}$$

  where

  $$F_* := \int_{-\infty}^{\infty} F_v(u_*(\xi), v_*)e^{c_*\xi}u_*'(\xi)\mathrm{d}\xi, \qquad G_* := G(u_*^+, v_*) - G(u_*^-, v_*) \tag{2.16}$$

  and $u_*^{\pm} := \lim_{\xi\to\pm\infty} u_*(\xi)$.
- **Intermediate regime:** $\frac{\bar{R}_0}{\delta} \leq \nu \leq \frac{r_0}{\delta^2}$. In this regime, to leading order

  $$\mathrm{sign}(\lambda_{\mathrm{c},2}) = \mathrm{sign}\left(-1 + \frac{M}{\delta^4\nu^3}\right), \tag{2.17}$$

  where $M = \mathcal{O}(1)$ with respect to δ, ν, and $\mathrm{sign}(M) = -\mathrm{sign}(F_*) \times \mathrm{sign}(G_*)$. In particular, if $M > 0$, then to leading order, $\lambda_{\mathrm{c},2}$ changes sign when $\nu \sim M^{1/3}\delta^{-4/3}$.
- **Strong advection regime:** $\nu \geq \frac{r_0}{\delta^2}$. Throughout this regime, to leading order we find that

  $$\mathrm{sign}(\lambda_{\mathrm{c},2}) = -1. \tag{2.18}$$

The asymptotic estimates are uniform in sufficiently small δ, so that the three regimes collectively describe the parameter region $\{(\delta,\nu) : 0 < \delta \leq \delta_0, 0 \leq \nu < \infty\}$ for some suitably small choice of $\delta_0 > 0$. In the weak advection regime, the stability of traveling fronts to long wavelength perturbations is encoded purely in the nonlinearities F and G, evaluated along the fast heteroclinic orbit $u_*(\xi)$. This criterion is analogous to that obtained in [14] in the absence of advection, and in the limit $\nu \to 0$ the corresponding expression for $\lambda_{c,2}$ agrees with that found in [14, section 2]. As ν increases relative to δ, in the intermediate regime, depending on the nonlinearities F and G and the relative size of ν with respect to δ, traveling fronts can be stable or unstable to long wavelength perturbations, with a potential sign change of $\lambda_{c,2}$ occurring at the critical scaling $\nu \sim \mathcal{O}(\delta^{-4/3})$. Finally, in the strong advection regime, all bistable traveling fronts considered here are stable to long wavelength perturbations. In this sense, the presence of advection has a stabilizing effect on the front as a planar interface.

To obtain the stability criteria above, we employ a mixture of geometric singular perturbation theory and formal asymptotic arguments to construct the adjoint solution $(u^A, v^A)(\xi)$ and estimate the expression (2.14) in each of the scaling regimes. However, we emphasize that the results above could, in principle, be obtained rigorously using geometric singular perturbation methods, in combination with exponential dichotomies/trichotomies, and Lin's method, or Evans function approaches; see, e.g., [5, 47] for thorough analyses of stability of planar traveling fronts and stripe solutions in specific reaction-diffusion-advection equations. However, for our purposes, we believe that such a technical analysis would detract from the simple message herein, that the presence of advection has a stabilizing effect on planar interfaces, and a straightforward stability criterion which can easily be applied in many example systems.

The remainder of this paper is outlined as follows. In section 3 we describe the construction of traveling fronts and the leading order computation of $\lambda_{c,2}$ in the weak advection and intermediate regimes, while the strong advection regime is considered in section 4. In section 5, we apply these results to an explicit dryland ecosystem model, and section 6 contains some numerical simulations and a brief discussion of the results.

3. Weak advection and intermediate regimes. Due to the similarity in the slow-fast geometry associated with the weak advection and intermediate regimes, in this section we consider both regimes, and outline the differences in each case. Taken together, we consider the regime $0 \leq \nu \leq \frac{r_0}{\delta^2}$, or equivalently, $0 \leq r \leq r_0$, where r_0 is a (yet to be fixed) small parameter. Therefore, we are interested in the behavior of the traveling wave equation (2.2) when both δ and $r = \delta^2\nu$ can be taken as small parameters.

This leads to a system with (up to) three timescales, and there is a distinction between the singular limits obtained by taking $\delta \to 0$ with r fixed, versus $r \to 0$ with δ fixed. Hence the case $0 \leq r \leq r_0$ needs to be split into two subcases: (i) $r = \bar{r}\delta, \bar{r} \leq \bar{R}_0$, corresponding to the weak advection regime and (ii) $\delta = \bar{\delta} r, \bar{\delta} \leq \bar{\delta}_0$, corresponding to the intermediate regime. We can then choose the quantities $\bar{R}_0, \bar{\delta}_0$ so that these regimes overlap, and we can understand the slow-fast structure of traveling fronts in the entire region $0 \leq r \leq r_0, 0 < \delta \leq \delta_0$ for some small $0 < r_0, \delta_0 \ll 1$.

We begin by describing the slow-fast structure of traveling fronts in each case in section 3.1, followed by a computation of the coefficient $\lambda_{c,2}$ in section 3.2.

3.1. Structure of traveling fronts. The structure of the orbits in each case is similar, but with a different parameter used as the timescale separation parameter

(δ versus r) in each case. We consider the first case in detail, and then outline differences relevant for the analysis of the second case.

3.1.1. Case (i): $r = \bar{r}\delta$, $0 \le \bar{r} \le \bar{R}_0$. We set $r = \bar{r}\delta$ in (2.3), obtaining

$$\begin{aligned} u_\xi &= p, \\ p_\xi &= -cp - F(u,v), \\ v_\xi &= \delta q, \\ q_\xi &= -\delta\left((\bar{r} + \delta c)q + G(u,v)\right). \end{aligned} \tag{3.1}$$

which we aim to analyze for all $0 \le \bar{r} \le \bar{R}_0$ for fixed $\bar{R}_0 > 0$, where $\bar{R}_0$ is a large constant which is $\mathcal{O}(1)$ with respect to δ. This results in a 2-fast-2-slow system with timescale separation parameter δ. Setting $\delta = 0$, we obtain the layer problem

$$\begin{aligned} u_\xi &= p, \\ p_\xi &= -cp - F(u,v). \end{aligned} \tag{3.2}$$

We recall, by Assumption 1, that the set $\mathcal{S} = \{F(u,v) = 0\}$ has two (different) branches $\mathcal{S}^\pm$ given by graphs $u = f^\pm(v)$ for $v \in I_v^\pm$, where $f^\pm(V^\pm) = U^\pm$. As the branches are defined away from points where $F_u = 0$, by Assumption 1(i), the quantity F_u has fixed (negative) sign on the branches $\mathcal{S}^\pm$. Therefore, the layer problem (3.2) admits two hyperbolic equilibria given by $u = f^\pm(v), p = 0$ for $v \in I_v^\pm$, respectively, so that (3.1) admits a 2D critical manifold $\mathcal{M}_0 := \{p = 0, F(u,v) = 0\}$, consisting of (at least) two branches

$$\mathcal{M}_0^- = \{p = 0, u = f^-(v), v \in I_v^-\}, \qquad \mathcal{M}_0^+ = \{p = 0, u = f^+(v), v \in I_v^+\}, \tag{3.3}$$

where $F(f^\pm(v), v) = 0$, and $V^- \in I_v^-$, $V^+ \in I_v^+$. Assumption 1(i) implies that $\mathcal{M}_0^\pm$ are of saddle type in their respective regions of definition. Using phase plane techniques, by appropriately adjusting the wave speed c if $I_v^- \cap I_v^+ \neq \emptyset$, then for any $v_* \in I_v^- \cap I_v^+$, there exists a locally unique speed c_* and corresponding heteroclinic orbit $u_*(\xi)$ between the saddle branches $\mathcal{M}_0^-$ and $\mathcal{M}_0^+$ lying in the intersection $\mathcal{W}^{\mathrm{u}}(\mathcal{M}_0^-) \cap \mathcal{W}^{\mathrm{s}}(\mathcal{M}_0^+)$; see Figure 3.

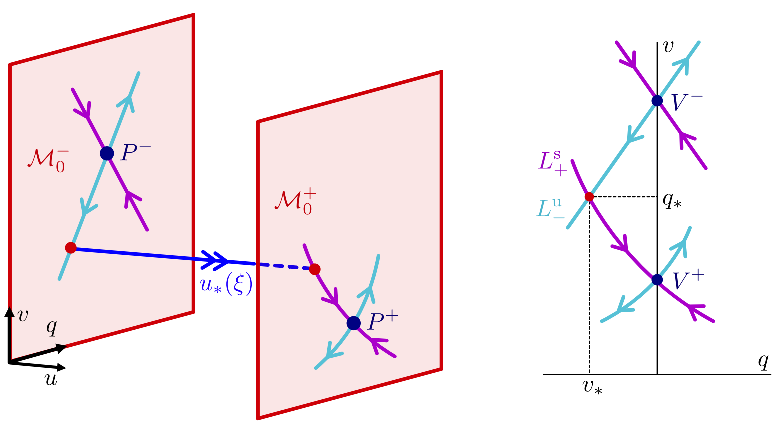

Fig. 3. *Shown is a schematic of the slow-fast construction of the singular traveling front in the weak advection regime. (Left) The fast jump $u_*(\xi)$ of the layer problem* (3.2) *between the manifolds $\mathcal{M}_0^\pm$ in (u,v,q)-space. (Right) Intersection of (projection of) manifolds L_-^{u} and L_+^{s} of the reduced flows* (3.6) *as in Assumption* 4.

We now rescale $\zeta = \delta\xi$ and consider the corresponding slow system

$$\begin{aligned} \delta u_\zeta &= p, \\ \delta p_\zeta &= -cp - F(u,v), \\ v_\zeta &= q, \\ q_\zeta &= -\left((\bar{r}+\delta c)q + G(u,v)\right). \end{aligned} \tag{3.4}$$

Setting $\delta = 0$, we obtain the corresponding reduced system

$$\begin{aligned} 0 &= p, \\ 0 &= -cp - F(u,v), \\ v_\zeta &= q, \\ q_\zeta &= -\left(\bar{r}q + G(u,v)\right). \end{aligned} \tag{3.5}$$

in which the flow is restricted to the critical manifold $\mathcal{M}_0$. The reduced flow on each of the saddle branches $\mathcal{M}_0^-$ and $\mathcal{M}_0^+$ is given by the planar flows

$$\begin{aligned} v_\zeta &= q, \\ q_\zeta &= -\left(\bar{r}q + G(f^\pm(v),v)\right), \end{aligned} \tag{3.6}$$

or equivalently, the scalar equations

$$v_{\zeta\zeta} + \bar{r}v_\zeta + G(f^\pm(v),v) = 0. \tag{3.7}$$

By Assumption 1(i), $(U^+,V^+) = (f^+(V^+),V^+)$ are fixed points of the full system. Since

$$(f^\pm)'(v) = -F_v(f^\pm(v),v)/F_u(f^\pm(v),v),$$

the conditions (2.4) imply that $G_u(f^\pm(V^\pm),V^\pm)(f^\pm)'(V^\pm) + G_v(f^\pm(V^\pm),V^\pm) < 0$, and hence $(v,q) = (V^\pm,0)$ correspond to saddle fixed points of the reduced flows (3.6) on $\mathcal{M}_0^\pm$, respectively. We denote by $L_\pm^{\mathrm{s,u}}$ the stable/unstable manifolds of the fixed points $(V^\pm,0)$. In this setting, to ensure the existence of a traveling front for $0 < \delta \ll 1$, we need to make the following assumption, which can be checked in a given system by examining the planar flows (3.6) for given $\bar{r}$ and nonlinearity $G(u,v)$ (see right panel of Figure 3).

Assumption 4. The projection of the manifold L_-^{u} from $\mathcal{M}_0^-$ onto $\mathcal{M}_0^+$ transversely intersects L_+^{s} at $(v,q) = (v_*,q_*)$ for some $v_* \in I_v^- \cap I_v^+$.

Considering the manifolds $L_\pm^{\mathrm{s,u}}$ as subsets of the critical manifold $\mathcal{M}_0$ and taking the union of their fast (un)stable fibers, we can construct the singular 2D stable and unstable manifolds of the equilibria $P^\pm$ in the full system as $\mathcal{W}^{\mathrm{s,u}}(P^\pm) := \mathcal{W}^{\mathrm{s,u}}(L_\pm^{\mathrm{s,u}}) \subset \mathcal{W}^{\mathrm{s,u}}(\mathcal{M}_0^\pm)$.

A singular heteroclinic orbit between the equilibria $P^\pm$ can then be formed by concatenating slow-fast trajectories from the layer/reduced problems as follows. The solution leaves P^- along the slow unstable manifold $L_-^{\mathrm{u}} \subset \mathcal{M}_0^-$, then departs $\mathcal{M}_0^-$ along a fast jump contained within $\mathcal{W}^{\mathrm{u}}(L_-^{\mathrm{u}})$ at the critical jump value $v = v_*$. Combining the analysis of the layer problem (3.2) above with Assumption 4, by choosing $c = c_*$ appropriately this fast jump forms a heteroclinic orbit which lies in the intersection $\mathcal{W}^{\mathrm{u}}(L_-^{\mathrm{u}}) \cap \mathcal{W}^{\mathrm{s}}(L_+^{\mathrm{s}})$. The orbit then tracks L_+^{s} until reaching P^+; see Figure 3. This sequence forms a singular orbit from which, for sufficiently small $\delta_0 > 0$, a solution to the full system (2.3) for $0 < \delta \le \delta_0$ with speed $c = c_* + \mathcal{O}(\delta)$ can be obtained using geometric singular perturbation theory.

3.1.2. Case (ii): $\boldsymbol{\delta = \bar\delta r}$, $\boldsymbol{0 < \bar\delta \le \bar\delta_0}$. We now consider $r \ll 1$ and set $\delta = \bar\delta r$ in (2.3), obtaining

$$
\begin{aligned}
u_\xi &= p,\\
p_\xi &= -cp - F(u,v),\\
v_\xi &= \bar\delta r q,\\
q_\xi &= -r\left((1+\bar\delta^2 rc)q + \bar\delta G(u,v)\right).
\end{aligned}
\tag{3.8}
$$

which we similarly aim to analyze for all $0 < \bar\delta < \bar\delta_0$ for any $\bar\delta_0 > 0$ where $\bar\delta_0$ is a small constant which is $\mathcal{O}(1)$ with respect to r. This system is now a 2-fast-2-slow system with timescale separation parameter r, and $\bar\delta$ as an additional small parameter. For $\bar\delta$ bounded away from zero, the analysis proceeds similarly as in the previous section. However, for sufficiently small $\bar\delta$, in order to obtain the precise form of the expression (2.17), we require more detailed estimates on the existence problem.

First, we rescale $q = \bar\delta\tilde q$ to obtain the system

$$
\begin{aligned}
u_\xi &= p,\\
p_\xi &= -cp - F(u,v),\\
v_\xi &= \bar\delta^2 r\tilde q,\\
\tilde q_\xi &= -r\left((1+\bar\delta^2 rc)\tilde q + G(u,v)\right).
\end{aligned}
\tag{3.9}
$$

Setting $\tau = r\xi$, we obtain the reduced flow for $r = 0$ on the manifolds $\mathcal{M}_0^\pm$

$$
\begin{aligned}
v_\tau &= \bar\delta^2\tilde q,\\
\tilde q_\tau &= -\tilde q - G(f^\pm(v),v),
\end{aligned}
\tag{3.10}
$$

which can be analyzed as planar slow-fast system with singular perturbation parameter $\bar\delta^2$. In particular, this allows us to easily determine the manifolds L_-^{u} and L_+^{s}. Note that in the limit $\bar\delta \to 0$, there exist normally attracting invariant manifolds $\mathcal{C}_0^\pm = \{\tilde q = -G(f^\pm(v),v)\} \subset \mathcal{M}_0^\pm$ with corresponding reduced flows

$$
v_{\tilde\tau} = -G(f^\pm(v),v),
\tag{3.11}
$$

where $\tilde\tau = \bar\delta^2\tau$. As argued in section 3.1.1, Assumption 1 implies that the quantities $\kappa_\pm := G_u(f^\pm(V^\pm),V^\pm)(f^\pm)'(V^\pm) + G_v(f^\pm(V^\pm),V^\pm) < 0$, and hence the fixed points $v = V^\pm$ are repelling within $\mathcal{C}_0^\pm$. Since the manifolds $\mathcal{C}_0^\pm$ are normally attracting in the reduced flow (3.10), they perturb to locally invariant manifolds $\mathcal{C}_{\bar\delta}^\pm$ for all sufficiently small $\bar\delta$, we deduce that the manifold L_-^{u} corresponds to the perturbed manifold $\mathcal{C}_{\bar\delta}^-$ given as a graph $\tilde q = -G(f^-(v),v) + \mathcal{O}(\bar\delta^2)$, and L_+^{s} corresponds to the perturbed stable fiber of $\mathcal{C}_{\bar\delta}^+$ which meets $\mathcal{C}_{\bar\delta}^+$ at $v = V^+$, and can be written as a graph $v = V^+ + \mathcal{O}(\bar\delta^2)$. For the manifolds L_+^{s} and L_-^{u} to intersect in their combined projection, as in Assumption 4, for all small $\bar\delta > 0$, they do so at a point $v_* = V^+ + \mathcal{O}(\bar\delta^2)$ and $\tilde q_* = \mathcal{O}(\bar\delta^2)$, which therefore defines the critical jump value and corresponding speed $c = c_*$ in the fast subsystem. Denoting by $v^\pm(\tau)$ the solutions corresponding to L_+^{s} and L_-^{u} satisfying $v^\pm(0) = v_*$, we have that

$$
\begin{aligned}
v_\tau^-(\tau) &= -\bar\delta^2 G(f^-(v^-(\tau)),v^-(\tau)) + \mathcal{O}(\bar\delta^4), \quad \tau < 0,\\
v_\tau^+(\tau) &= \mathcal{O}(\bar\delta^4), \quad \tau > 0,
\end{aligned}
\tag{3.12}
$$

and $v_\tau^+(\tau)$ decays with exponential rate $-1 + \bar\delta^2\kappa_+$ to leading order as $\tau \to \infty$.

Remark 3.1. Assuming $V^- > V^+$, without loss of generality, we note that to ensure that Assumption 4 holds for all sufficiently small $\bar\delta$, it suffices to assume that

$G(f^-(v),v)<0$ for all $v\in[V^+,V^-)$. This connects the structure of the existence problem in the intermediate regime to that in the strong advection regime; see section 4.1 and Assumption 5.

Using this construction in the region of small $\bar{\delta}$, we therefore obtain singular heteroclinic orbits for all $0<\bar{\delta}<\bar{\delta}_0$, which can be shown, using geometric singular perturbation techniques to perturb to traveling front solutions with speed $c=c_*+\mathcal{O}(r)$ for all $0<r<r_0$ for some $r_0\ll 1$. Fixing $\bar{\delta}_0$ sufficiently small above, and taking $\bar{R}_0>\bar{\delta}_0^{-1}$ in section 3.1.1, and possibly taking r_0 and/or δ_0 smaller if necessary, we can combine these results with those of the previous section to obtain a slow-fast description of singular traveling fronts for any $0\le r\le r_0, 0<\delta\le\delta_0$. The boundary between the weak and intermediate regimes occurs when $r=\mathcal{O}(\delta)$, or equivalently, when $\nu=\mathcal{O}(\delta^{-1})$.

3.2. Long wavelength (in)stability: Leading order computation of $\boldsymbol{\lambda_{c,2}}$. Given the slightly different slow-fast structures of the weak advection and intermediate regimes in section 3.1, we similarly separate the computation of $\lambda_{c,2}$ in each case, depending on whether δ or r is used as the primary singular perturbation parameter. In each case, the goal is to approximate (2.14) by obtaining leading order expressions for the adjoint solution $(u^A,v^A)(\xi)$ in the corresponding fast and slow fields.

3.2.1. Case (i): $\boldsymbol{r=\bar{r}\delta,\ 0\le\bar{r}\le\bar{R}_0}$. We consider the fast

$$\begin{aligned}u_{\xi\xi}-cu_\xi+F_u(u_{\mathrm{h}}(\xi),v_{\mathrm{h}}(\xi))u+G_u(u_{\mathrm{h}}(\xi),v_{\mathrm{h}}(\xi))v&=0,\\ v_{\xi\xi}-\left(\bar{r}\delta+\delta^2c\right)v_\xi+\delta^2F_v(u_{\mathrm{h}}(\xi),v_{\mathrm{h}}(\xi))u+\delta^2G_v(u_{\mathrm{h}}(\xi),v_{\mathrm{h}}(\xi))v&=0\end{aligned}\tag{3.13}$$

and slow

$$\begin{aligned}\delta^2u_{\zeta\zeta}-\delta cu_\zeta+F_u(u_{\mathrm{h}}(\zeta/\delta),v_{\mathrm{h}}(\zeta/\delta))u+G_u(u_{\mathrm{h}}(\zeta/\delta),v_{\mathrm{h}}(\zeta/\delta))v&=0,\\ v_{\zeta\zeta}-(\bar{r}+\delta c)v_\zeta+F_v(u_{\mathrm{h}}(\zeta/\delta),v_{\mathrm{h}}(\zeta/\delta))u+G_v(u_{\mathrm{h}}(\zeta/\delta),v_{\mathrm{h}}(\zeta/\delta))v&=0\end{aligned}\tag{3.14}$$

formulations of the adjoint equation (2.12). In the fast field, to leading order $u_{\mathrm{h}}(\xi)=u_*(\xi), v_{\mathrm{h}}(\xi)=v_*$, and $c=c_*$, so that to leading order the fast system is given by

$$\begin{aligned}u_{\xi\xi}-c_*u_\xi+F_u(u_*(\xi),v_*)u+G_u(u_*(\xi),v_*)v&=0,\\ v_{\xi\xi}&=0\end{aligned}\tag{3.15}$$

from which we deduce that $v=\bar{v}_*=$ constant and u satisfies

$$u_{\xi\xi}-c_*u_\xi+F_u(u_*(\xi),v_*)u=-G_u(u_*(\xi),v_*)\bar{v}_*.\tag{3.16}$$

The left-hand side of (3.16) can be written as $\mathcal{L}_*^Au$, where

$$\mathcal{L}_*^A:=\partial_{\xi\xi}-c_*\partial_\xi+F_u(u_*(\xi),v_*)\tag{3.17}$$

is the adjoint of the linearization

$$\mathcal{L}_*:=\partial_{\xi\xi}+c_*\partial_\xi+F_u(u_*(\xi),v_*)\tag{3.18}$$

of the reduced system (2.5) along the fast jump. The kernel of $\mathcal{L}_*$ is spanned by the derivative $u_*'(\xi)$ of the fast heteroclinic orbit $u_*(\xi)$, while $u_*'(\xi)e^{c_*\xi}$ is the bounded solution of the adjoint equation $\mathcal{L}_*^Au=0$. Taking the inner product of (3.16) with $u_*'(\xi)$ implies that

$$0=\bar{v}_*\int_{-\infty}^{\infty}G_u(u_*(\xi),v_*)u_*'(\xi)\mathrm{d}\xi=\bar{v}_*\left(G(u_*^+,v_*)-G(u_*^-,v_*)\right).\tag{3.19}$$

By Assumption 3, $G(u_*^+, v_*) \neq G(u_*^-, v_*)$ so that $\bar{v}_* = 0$, and to leading order $v = 0$ and $u = \alpha_* u_*'(\xi) e^{c_* \xi}$.

For the slow system, we denote by $v^{\pm}(\zeta)$ the slow orbits of (3.6) corresponding to L_-^{u} and L_+^{s}, respectively, which satisfy $v^{\pm}(0) = v_*$. At leading order we find that

$$\begin{aligned} F_u(f^{\pm}(v^{\pm}), v^{\pm}) u + G_u(f^{\pm}(v^{\pm}), v^{\pm}) v &= 0, \\ v_{\zeta\zeta} - \bar{r} v_\zeta + F_v(f^{\pm}(v^{\pm}), v^{\pm}) u + G_v(f^{\pm}(v^{\pm}), v^{\pm}) v &= 0, \end{aligned} \tag{3.20}$$

or equivalently,

$$v_{\zeta\zeta} - \bar{r} v_\zeta + \left(G_v(f^{\pm}(v^{\pm}), v^{\pm}) - F_v(f^{\pm}(v^{\pm}), v^{\pm}) \frac{G_u(f^{\pm}(v^{\pm}), v^{\pm})}{F_u(f^{\pm}(v^{\pm}), v^{\pm})} \right) v = 0, \tag{3.21}$$

from which we deduce that $v^{A,\pm}(\zeta) = \delta \alpha^{\pm} e^{\bar{r}\zeta} v_\zeta^{\pm}(\zeta)$. To match along the fast jump, we note that to ensure continuity of v^A, we require $\alpha^+ = \alpha^- = \alpha$ since $v_\zeta^+(0) = q_* = v_\zeta^-(0)$. There is an offset in v_ζ^A from the slow equations across the fast jump since by (3.7) we have

$$\left[(e^{\bar{r}\zeta} v_\zeta^+(\zeta))_\zeta - (e^{\bar{r}\zeta} v_\zeta^-(\zeta))_\zeta \right]_{\zeta=0} = v_{\zeta\zeta}^+(0) - v_{\zeta\zeta}^-(0) = -\left(G(u_*^+, v_*) - G(u_*^-, v_*) \right), \tag{3.22}$$

so that

$$\begin{aligned} v_\xi^{A,+}(0) - v_\xi^{A,-}(0) &= \delta \left(v_\zeta^{A,+}(0) - v_\zeta^{A,-}(0) \right) = \delta^2 \alpha \left(v_{\zeta\zeta}^+(0) - v_{\zeta\zeta}^-(0) \right) \\ &= -\delta^2 \alpha \left(G(u_*^+, v_*) - G(u_*^-, v_*) \right). \end{aligned} \tag{3.23}$$

We therefore require a corresponding jump through the fast field. Integrating (3.13) over the fast field, and recalling that to leading order $v = \bar{v}_* = 0$, and $u = \alpha_* u_*'(\xi) e^{c_* \xi}$, we have to leading order

$$\begin{aligned} \Delta v_\xi^A &= \delta^2 \bar{r} \left(v_\zeta^+(0) - v_\zeta^-(0) \right) - \delta^2 \alpha_* \int_{-\infty}^{\infty} F_v(u_*(\xi), v_*) e^{c_* \xi} u_*'(\xi) \mathrm{d}\xi \\ &= -\delta^2 \alpha_* \int_{-\infty}^{\infty} F_v(u_*(\xi), v_*) e^{c_* \xi} u_*'(\xi) \mathrm{d}\xi, \end{aligned} \tag{3.24}$$

which, upon equating (3.23) and (3.24), we deduce that

$$\alpha = \alpha_* \frac{\int_{-\infty}^{\infty} F_v(u_*(\xi), v_*) e^{c_* \xi} u_*'(\xi) \mathrm{d}\xi}{G(u_*^+, v_*) - G(u_*^-, v_*)}. \tag{3.25}$$

We now compute

$$\begin{aligned} &\int_{-\infty}^{\infty} v_{\mathrm{h}}'(\xi) v^A(\xi) \mathrm{d}\xi \\ &= \int_{-\infty}^{-\frac{1}{\sqrt{\delta}}} v_{\mathrm{h}}'(\xi) v^A(\xi) \mathrm{d}\xi + \int_{-\frac{1}{\sqrt{\delta}}}^{\frac{1}{\sqrt{\delta}}} v_{\mathrm{h}}'(\xi) v^A(\xi) \mathrm{d}\xi + \int_{\frac{1}{\sqrt{\delta}}}^{\infty} v_{\mathrm{h}}'(\xi) v^A(\xi) \mathrm{d}\xi \\ &= \alpha \int_{-\infty}^{-\sqrt{\delta}} \delta e^{\bar{r}\zeta} v_\zeta^-(\zeta)^2 \mathrm{d}\zeta + \alpha \int_{-\frac{1}{\sqrt{\delta}}}^{\frac{1}{\sqrt{\delta}}} \delta^2 q_*^2 \mathrm{d}\xi + \alpha \int_{\sqrt{\delta}}^{\infty} \delta e^{\bar{r}\zeta} v_\zeta^+(\zeta)^2 \mathrm{d}\zeta + \mathcal{O}(\alpha\delta^2) \\ &= \alpha \int_{-\infty}^{-\sqrt{\delta}} \delta e^{\bar{r}\zeta} v_\zeta^-(\zeta)^2 \mathrm{d}\zeta + \alpha \int_{\sqrt{\delta}}^{\infty} \delta e^{\bar{r}\zeta} v_\zeta^+(\zeta)^2 \mathrm{d}\zeta + \mathcal{O}(\alpha\delta^{3/2}), \end{aligned}$$

and similarly,

$$\int_{-\infty}^{\infty} u_{\mathrm{h}}'(\xi) u^A(\xi) \mathrm{d}\xi = \alpha_* \left(\int_{-\infty}^{\infty} e^{c_* \xi} u_*'(\xi)^2 \mathrm{d}\xi + \mathcal{O}(\delta) \right)$$

so that to leading order, we estimate (2.14) as

(3.26)

$$\lambda_{\mathrm{c},2} \sim -\frac{1}{\delta} \frac{\int_{-\infty}^{\infty} F_v(u_*(\xi), v_*) e^{c_* \xi} u_*'(\xi) \mathrm{d}\xi}{G(u_*^+, v_*) - G(u_*^-, v_*)} \frac{\left(\int_{-\infty}^{0} e^{\bar{r}\zeta} v_\zeta^-(\zeta)^2 \mathrm{d}\zeta + \int_0^\infty e^{\bar{r}\zeta} v_\zeta^+(\zeta)^2 \mathrm{d}\zeta \right)}{\int_{-\infty}^{\infty} e^{c_* \xi} u_*'(\xi)^2 \mathrm{d}\xi}.$$

The last factor has fixed sign so that we immediately obtain the stability criterion (2.15) in the weak advection regime in terms of the quantities (2.16). The leading order asymptotic formula (3.26) holds provided $r = \bar{r}\delta, 0 \le \bar{r} \le \bar{R}_0, 0 < \delta \le \delta$, or in terms of ν, provided $0 \le \nu \le \frac{\bar{R}_0}{\delta}$. We note that the case $\nu = 0$ corresponds to setting $\bar{r} = 0$ in (3.26), which matches the expression obtained for the cofficient $\lambda_{\mathrm{c},2}$ in the absence of advection in [14, section 2].

3.2.2. Case (ii): $\boldsymbol{\delta = \bar{\delta} r}$, $\boldsymbol{0 < \bar{\delta} \le \bar{\delta}_0}$. We again consider the fast

$$\begin{aligned} u_{\xi\xi} - c u_\xi + F_u(u_{\mathrm{h}}(\xi), v_{\mathrm{h}}(\xi)) u + G_u(u_{\mathrm{h}}(\xi), v_{\mathrm{h}}(\xi)) v &= 0, \\ v_{\xi\xi} - \left(r + \bar{\delta}^2 r^2 c \right) v_\xi + \bar{\delta}^2 r^2 F_v(u_{\mathrm{h}}(\xi), v_{\mathrm{h}}(\xi)) u + \bar{\delta}^2 r^2 G_v(u_{\mathrm{h}}(\xi), v_{\mathrm{h}}(\xi)) v &= 0 \end{aligned} \tag{3.27}$$

and slow

(3.28)

$$\begin{aligned} r^2 u_{\tau\tau} - r c u_\tau + F_u(u_{\mathrm{h}}(\tau/r), v_{\mathrm{h}}(\tau/r)) u + G_u(u_{\mathrm{h}}(\tau/r), v_{\mathrm{h}}(\tau/r)) v &= 0, \\ v_{\tau\tau} - \left(1 + \bar{\delta}^2 r c \right) v_\tau + \bar{\delta}^2 F_v(u_{\mathrm{h}}(\tau/r), v_{\mathrm{h}}(\tau/r)) u + \bar{\delta}^2 G_v(u_{\mathrm{h}}(\tau/r), v_{\mathrm{h}}(\tau/r)) v &= 0 \end{aligned}$$

formulations of the adjoint equation. At leading order the fast system is given by

$$\begin{aligned} u_{\xi\xi} - c_* u_\xi + F_u(u_*(\xi), v_*) u + G_u(u_*(\xi), v_*) v &= 0, \\ v_{\xi\xi} &= 0 \end{aligned} \tag{3.29}$$

from which we deduce as in section 3.2.1 that to leading order $v = 0$ and $u(\xi) = \alpha_* e^{c_* \xi} u_*'(\xi)$. For the slow system, recalling that $v^\pm(\tau)$ denote the solutions of (3.10) corresponding to L_+^{s} and L_-^{u} satisfying $v^\pm(0) = v_*$, at leading order we find that

$$\begin{aligned} F_u(f^\pm(v^\pm), v^\pm) u + G_u(f^\pm(v^\pm), v^\pm) v &= 0, \\ v_{\tau\tau} - v_\tau + \bar{\delta}^2 F_v(f^\pm(v^\pm), v^\pm) u + \bar{\delta}^2 G_v(f^\pm(v^\pm), v^\pm) v &= 0, \end{aligned} \tag{3.30}$$

or equivalently,

$$v_{\tau\tau} - v_\tau + \bar{\delta}^2 \left(G_v(f^\pm(v^\pm), v^\pm) - F_v(f^\pm(v^\pm), v^\pm) \frac{G_u(f^\pm(v^\pm), v^\pm)}{F_u(f^\pm(v^\pm), v^\pm)} \right) v = 0, \tag{3.31}$$

from which we deduce that $v^{A,\pm}(\tau) = r\alpha^\pm e^\tau v_\tau^\pm(\tau)$ in the slow fields. To match along the fast jump, we note that to ensure continuity of v^A, we require $\alpha^+ = \alpha^- = \alpha$ since $v_\tau^+(0) = v_\tau^-(0)$. Proceeding as in section 3.2.1, to account for the jump in v_τ^A from the slow equations across the fast jump

(3.32)

$$\left[(e^\tau v_\tau^+(\tau))_\tau - (e^\tau v_\tau^-(\tau))_\tau \right]_{\tau=0} = v_{\tau\tau}^+(0) - v_{\tau\tau}^-(0) = -\bar{\delta}^2 \left(G(u_*^+, v_*) - G(u_*^-, v_*) \right),$$

we require a corresponding jump through the fast field

$$\Delta v_\xi^A = -\bar{\delta}^2 r^2 \alpha_* \int_{-\infty}^{\infty} F_v(u_*(\xi), v_*) e^{c_*\xi} u_*'(\xi) \mathrm{d}\xi = r^2\alpha \left(v_{\tau\tau}^+(0) - v_{\tau\tau}^-(0) \right), \tag{3.33}$$

which implies

$$\alpha = \alpha_* \frac{\int_{-\infty}^{\infty} F_v(u_*(\xi), v_*) e^{c_*\xi} u_*'(\xi) \mathrm{d}\xi}{G(u_*^+, v_*) - G(u_*^-, v_*)}. \tag{3.34}$$

Using the estimates of section 3.1.2, we similarly proceed as in section 3.2.1 and estimate

$$\begin{aligned}
\int_{-\infty}^{\infty} v_{\mathrm{h}}'(\xi) v^A(\xi) \mathrm{d}\xi &= \int_{-\infty}^{-\frac{1}{\sqrt{r}}} v_{\mathrm{h}}'(\xi) v^A(\xi) \mathrm{d}\xi + \int_{-\frac{1}{\sqrt{r}}}^{\frac{1}{\sqrt{r}}} v_{\mathrm{h}}'(\xi) v^A(\xi) \mathrm{d}\xi + \int_{\frac{1}{\sqrt{r}}}^{\infty} v_{\mathrm{h}}'(\xi) v^A(\xi) \mathrm{d}\xi \\
&= \alpha \int_{-\infty}^{-\sqrt{r}} r e^{\tau} v_\tau^-(\tau)^2 \mathrm{d}\tau + \alpha \int_{\sqrt{r}}^{\infty} r e^{\tau} v_\tau^+(\tau)^2 \mathrm{d}\tau + \mathcal{O}(\alpha \bar{\delta}^4 r^{3/2}) \\
&= \alpha r \bar{\delta}^4 \left(\int_{-\infty}^{0} e^{\tau} G(f^-(v^-(\tau)), v^-(\tau))^2 \mathrm{d}\tau + \mathcal{O}(\bar{\delta}^2, \sqrt{r}) \right) \\
\int_{-\infty}^{\infty} u_{\mathrm{h}}'(\xi) u^A(\xi) \mathrm{d}\xi &= \alpha_* \left(\int_{-\infty}^{\infty} e^{c_*\xi} u_*'(\xi)^2 \mathrm{d}\xi + \mathcal{O}(r) \right),
\end{aligned}$$

where we used the estimate (3.12) and the fact that $\bar{\delta} \le \bar{\delta}_0$ is small. We now estimate (2.14) to leading order as

$$\begin{aligned}
\lambda_{\mathrm{c},2} &\sim -1 - \frac{\alpha r \bar{\delta}^4}{\alpha_* \delta^2} \frac{\left(\int_{-\infty}^{0} e^{\tau} G(f^-(v^-(\tau)), v^-(\tau))^2 \mathrm{d}\tau + \mathcal{O}(\bar{\delta}^2, \sqrt{r}) \right)}{\int_{-\infty}^{\infty} e^{c_*\xi} u_*'(\xi)^2 \mathrm{d}\xi} \\
&= -1 - \frac{\bar{\delta}^2}{r} \frac{\int_{-\infty}^{\infty} F_v(u_*(\xi), v_*) e^{c_*\xi} u_*'(\xi) \mathrm{d}\xi}{G(u_*^+, v_*) - G(u_*^-, v_*)} \frac{\left(\int_{-\infty}^{0} e^{\tau} G(f^-(v^-(\tau)), v^-(\tau))^2 \mathrm{d}\tau \right)}{\int_{-\infty}^{\infty} e^{c\xi} u_f'(\xi)^2 \mathrm{d}\xi} \\
&\quad + \mathcal{O}\left(\frac{\bar{\delta}^2}{\sqrt{r}}, \frac{\bar{\delta}^4}{r} \right).
\end{aligned} \tag{3.35}$$

From this, we obtain the stability criterion (2.17) in the intermediate regime. The leading order expression (2.17) is valid provided $\delta = \bar{\delta} r, 0 < \bar{\delta} \le \bar{\delta}_0, 0 \le r \le r_0$, or in terms of ν, provided $\frac{1}{\bar{\delta}_0 \delta} \le \nu \le \frac{r_0}{\delta^2}$; since $\bar{R}_0 > \bar{\delta}_0^{-1}$, this similarly holds for ν satisfying $\frac{\bar{R}_0}{\delta} \le \nu \le \frac{r_0}{\delta^2}$. We see that the first (constant) term -1 dominates when $\bar{\delta}^2 \ll r$, while the second term dominates when $r \ll \bar{\delta}^2$. If the coefficient of the latter is positive, then the expression (3.35) changes sign when

$$r = -\bar{\delta}^2 \frac{\int_{-\infty}^{\infty} F_v(u_*(\xi), v_*) e^{c_*\xi} u_*'(\xi) \mathrm{d}\xi}{G(u_*^+, v_*) - G(u_*^-, v_*)} \frac{\int_{-\infty}^{0} e^{\tau} G(f^-(v^-(\tau)), v^-(\tau))^2 \mathrm{d}\tau}{\int_{-\infty}^{\infty} e^{c_*\xi} u_*'(\xi)^2 \mathrm{d}\xi} + \mathcal{O}\left(\bar{\delta}^4\right),$$

or equivalently, when

$$\nu = M^{1/3} \delta^{-4/3} \left(1 + \mathcal{O}(\delta^{2/3}) \right),$$

where

$$M := \frac{-\int_{-\infty}^{\infty} F_v(u_*(\xi), v_*) e^{c_*\xi} u_*'(\xi) \mathrm{d}\xi}{G(u_*^+, v_*) - G(u_*^-, v_*)} \frac{\int_{-\infty}^{0} e^{\tau} G(f^-(v^-(\tau)), v^-(\tau))^2 \mathrm{d}\tau}{\int_{-\infty}^{\infty} e^{c_*\xi} u_*'(\xi)^2 \mathrm{d}\xi}. \tag{3.36}$$

We emphasize that the sign of M is determined by the same quantities F_*, G_* defined in (2.16) which determine the sign of $\lambda_{\mathrm{c},2}$ in the weak advection regime.

4. Strong advection regime. We now determine the behavior of the system in the strong advection regime for $r \geq r_0$, where r_0 is the small constant from section 3, or equivalently, for $\nu \geq \frac{r_0}{\delta^2}$.

4.1. Slow-fast structure of the traveling front. We rescale $q = \frac{\delta}{r}\tilde{q}$ and obtain

$$\begin{aligned} u_\xi &= p, \\ p_\xi &= -cp - F(u,v), \\ v_\xi &= \varepsilon \tilde{q}, \\ \tilde{q}_\xi &= r\left(-(1+\varepsilon c)\,\tilde{q} - G(u,v)\right), \end{aligned} \tag{4.1}$$

where we recall $\varepsilon := \nu^{-1} = \frac{\delta^2}{r}$. We now consider this equation in the regime $0 < \varepsilon \ll 1$ and $r \geq r_0$. We use ε as the timescale separation parameter, so that v is a slow variable, and $(u,p,\tilde{q})$ are fast variables. We note that if r is large, then $\tilde{q}$ evolves on a third ("super" fast) timescale; see below. Setting $\varepsilon = 0$ defines the layer problem

$$\begin{aligned} u_\xi &= p, \\ p_\xi &= -cp - F(u,v), \\ \tilde{q}_\xi &= -r\left(\tilde{q} + G(u,v)\right), \end{aligned} \tag{4.2}$$

and the critical manifold

$$\tilde{\mathcal{M}}_0 := \{p = 0, F(u,v) = 0, \tilde{q} = -G(u,v)\}, \tag{4.3}$$

which admits at least two normally hyperbolic branches $\tilde{\mathcal{M}}_0^\pm = \{p = 0, u = f^\pm(v), \tilde{q} = -G(f^\pm(v),v)\}$. The reduced flow on these manifolds is given by

$$v_\eta = -G(f^\pm(v),v) \tag{4.4}$$

with respect to $\eta = \varepsilon\xi$. By Assumption 1, $G_u(f^\pm(V^\pm),V^\pm)(f^\pm)'(V^\pm) + G_v(f^\pm(V^\pm), V^\pm) < 0$, so that the equilibria $v = V^\pm$ are repelling on $\tilde{\mathcal{M}}_0^\pm$. We assume the following.

Assumption 5. Without loss of generality, we assume $V^- > V^+$ and that $[V^+, V^-] \subseteq I_v^-$. Furthermore, $G(f^-(v),v) < 0$ for $v \in [V^+, V^-)$.

In this case, the unstable manifold of the equilibrium $v = V^-$ in the reduced flow (4.4) includes the segment $\tilde{\mathcal{M}}_0^- \cap \{V^+ \leq v < V^-\}$, consisting of a single solution; we denote by $v = v^-(\eta)$ the corresponding solution satisfying $v^-(0) = V^+$. On the other hand, the stable manifold of $v = V^+$ in the reduced flow (4.4) on $\tilde{\mathcal{M}}_0^+$ is trivial; see Figure 4. Thus, to form a singular heteroclinic orbit between $P^\pm$ in the full system, it is necessary for the fast jump to occur in the subspace $v = V^+$, which can be arranged by taking $v_* = V^+$, and choosing c_* appropriately to obtain a fast heteroclinic orbit $(u_*, p_*)(\xi)$ in the (u,p)-subsystem of the layer problem

$$\begin{aligned} u_\xi &= p, \\ p_\xi &= -cp - F(u,v_*). \end{aligned} \tag{4.5}$$

The associated $\tilde{q}$-profile can then be obtained by integrating

$$\tilde{q}_*(\xi) = -r\int_{-\infty}^{\xi} e^{-r(\xi-\tilde{\xi})} G(u_*(\tilde{\xi}), v_*)\mathrm{d}\tilde{\xi}. \tag{4.6}$$

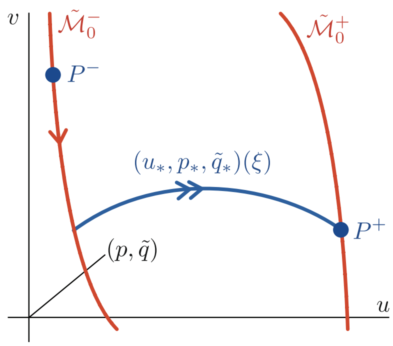

FIG. 4. *Schematic of the slow-fast construction of the singular traveling front in the strong advection regime.*

We note that the additional fast direction adds a uniformly stable hyperbolic direction to each of the critical manifolds $\tilde{\mathcal{M}}_0^0$, $\tilde{\mathcal{M}}_0^+$, and hence just adds $+1$ to the dimension of their respective stable manifolds. The resulting construction is valid for any value of r which is $\mathcal{O}(1)$ with respect to ε.

To make this construction well-defined in the limit $r \to \infty$ (so that we obtain a slow-fast description of the traveling front for all $r \geq r_0$ and $\varepsilon \leq \varepsilon_0$ for some ε_0 independent of r), we note that for large $r \gg 1$, the system (4.1) is a slow-fast system with timescale separation parameter $\rho := 1/r$, with one fast variable $\tilde{q}$ and three slow variables (u, p, v). For $\rho = 0$, the system admits a three-dimensional normally hyperbolic critical manifold

$$\mathcal{Q}_0 = \left\{ \tilde{q} = Q_0(u, p, v; \varepsilon) = -\frac{G(u, v)}{1 + \varepsilon c} \right\}, \tag{4.7}$$

which perturbs for all sufficiently small $\rho > 0$ to a normally hyperbolic slow manifold

$$\mathcal{Q}_\rho = \left\{ \tilde{q} = Q_\rho(u, p, v; \varepsilon) = -\frac{G(u, v)}{1 + \varepsilon c} + \mathcal{O}(\rho) \right\}, \tag{4.8}$$

where we note that

$$Q_\rho(f^\pm(v), 0, v; 0) = -G(f^\pm(v), v) \tag{4.9}$$

for all ρ since when $\varepsilon = 0$, the sets $\{(u, p, v, \tilde{q}) = (f^\pm(v), 0, v, -G(f^\pm(v), v))\}$ define curves of fixed points of (4.1). The flow on $\mathcal{Q}_\rho$ is given by

$$\begin{aligned} u_\xi &= p, \\ p_\xi &= -cp - F(u, v), \\ v_\xi &= \varepsilon Q_\rho(u, p, v; \varepsilon), \end{aligned} \tag{4.10}$$

which is itself a slow-fast system with timescale separation parameter ε. For $\varepsilon = 0$, this system admits critical manifolds which, in light of (4.9), are again given by $\tilde{\mathcal{M}}_0^\pm$ in the four-dimensional ambient space. The corresponding layer problem is given by (4.5), while the reduced problem on $\tilde{\mathcal{M}}_0^\pm$ is given by (4.4), again using (4.9). The construction of slow-fast traveling fronts in the full system (4.1) therefore proceeds similarly as above for all sufficiently small $\varepsilon > 0$, with the resulting orbits lying entirely within the invariant manifold $\mathcal{Q}_\rho$.

Putting together the results of this section, the slow-fast structure of traveling fronts is therefore well defined for any sufficiently small ε, and any $r \geq r_0$. However, due to the relations between the parameters $r, \delta, \varepsilon, \nu$, this region includes all $\nu \geq \frac{r_0}{\delta^2}$, $0 < \delta \leq \delta_0$, where the constant δ_0 from section 3 may be taken smaller, if necessary.

4.2. Long wavelength stability: Leading-order computation of $\boldsymbol{\lambda_{c,2}}$. We now consider the fronts from section 4.1, using ε as the timescale separation parameter. We consider the fast

$$\begin{aligned} u_{\xi\xi} - cu_\xi + F_u(u_\mathrm{h}(\xi), v_\mathrm{h}(\xi))u + G_u(u_\mathrm{h}(\xi), v_\mathrm{h}(\xi))v = 0,\\ \frac{1}{r}v_{\xi\xi} - (1+\varepsilon c)\, v_\xi + \varepsilon F_v(u_\mathrm{h}(\xi), v_\mathrm{h}(\xi))u + \varepsilon G_v(u_\mathrm{h}(\xi), v_\mathrm{h}(\xi))v = 0 \end{aligned} \tag{4.11}$$

and slow

$$\begin{aligned} \varepsilon^2 u_{\eta\eta} - \varepsilon c u_\eta + F_u(u_\mathrm{h}(\eta/\varepsilon), v_\mathrm{h}(\eta/\varepsilon))u + G_u(u_\mathrm{h}(\eta/\varepsilon), v_\mathrm{h}(\eta/\varepsilon))v = 0,\\ \frac{\varepsilon}{r}v_{\eta\eta} - (1+\varepsilon c)\, v_\eta + F_v(u_\mathrm{h}(\eta/\varepsilon), v_\mathrm{h}(\eta/\varepsilon))u + G_v(u_\mathrm{h}(\eta/\varepsilon), v_\mathrm{h}(\eta/\varepsilon))v = 0 \end{aligned} \tag{4.12}$$

formulations of the adjoint equation, where $\eta = \varepsilon\xi$. Proceeding as in section 3.2.1, in the fast field, to leading order $u_\mathrm{h}(\xi) = u_*(\xi), v_\mathrm{h}(\xi) = v_*$, and $c = c_*$, so that $v = \bar{v}_* =$ constant and u satisfies

$$u_{\xi\xi} - c_* u_\xi + F_u(u_*(\xi), v_*)u = -G_u(u_*(\xi), v_*)\bar{v}_*, \tag{4.13}$$

which implies that

$$0 = \bar{v}_* \int_{-\infty}^{\infty} G_u(u_*(\xi), v_*)u_*'(\xi)\mathrm{d}\xi = \bar{v}_* \left(G(u_*^+, v_*) - G(u_*^-, v_*)\right), \tag{4.14}$$

By Assumption 3, $G(u_*^+, v_*) \neq G(u_*^-, v_*)$ so that $\bar{v}_* = 0$ to leading order, and $u = \alpha_* u_*'(\xi)e^{c_*\xi}$. For the slow field, we recall that there is only a slow field along $\mathcal{M}_0^-$, on which $v = v^-(\eta)$ denotes the solution of (4.4) satisfying $v^-(0) = V^+$. Hence, to leading order, the adjoint equation reads

$$\begin{aligned} F_u(f^-(v^-), v^-)u + G_u(f^-(v^-), v^-)v = 0,\\ -v_\eta + F_v(f^-(v^-), v^-)u + G_v(f^-(v^-), v^-)v = 0, \end{aligned} \tag{4.15}$$

or equivalently,

$$-v_\eta + \left(G_v(f^-(v^-), v^-) - F_v(f^-(v^-), v^-)\frac{G_u(f^-(v^-), v^-)}{F_u(f^-(v^-), v^-)}\right)v = 0, \tag{4.16}$$

so that, in light of (4.4), to leading order $v(\eta) = \alpha^- v_\eta^-(\eta)^{-1}$ in the slow field, from which we deduce that $\alpha^- = 0$ and hence $v(\eta) = \mathcal{O}(\varepsilon)$ in the slow field. Thus, we obtain (at leading order)

$$\lambda_{c,2} = -\frac{\int_{-\infty}^{\infty} \alpha_* u_*'(\xi)^2 e^{c_*\xi}\mathrm{d}\xi}{\int_{-\infty}^{\infty} \alpha_* u_*'(\xi)^2 e^{c_*\xi}\mathrm{d}\xi} + \mathcal{O}\left(\frac{\varepsilon}{r}\right) = -1 + \mathcal{O}\left(\frac{\varepsilon}{r}\right),$$

which directly implies (2.18).

5. Application to a dryland ecosystem model. We apply the results of sections 3–4 to the following modified Klausmeier model [35] in the specific form introduced in [5]:

$$
\begin{aligned}
U_t &= \Delta U - \mu_1 U + U^2 V\left(1 - \mu_2 U\right), \\
V_t &= \frac{1}{\delta^2}\Delta V + \mu_3 - V - U^2 V + \nu V_x,
\end{aligned}
\tag{5.1}
$$

corresponding to (1.1) with $\boldsymbol{\mu} = (\mu_1, \mu_2, \mu_3)$ and

$$
\begin{aligned}
F(U, V; \boldsymbol{\mu}) &= -\mu_1 U + U^2 V\left(1 - \mu_2 U\right), \\
G(U, V; \boldsymbol{\mu}) &= \mu_3 - V - U^2 V.
\end{aligned}
\tag{5.2}
$$

In the context of dryland ecosystem U represents biomass of a species of vegetation, while V represents a limiting resource such as water. The model (5.1) also corresponds to that considered in [22] in the case of a single species. The system parameters μ_1, μ_2, μ_3 are positive and represent mortality, inverse of soil carrying capacity, and rainfall, respectively. The small parameter $0 < \delta \ll 1$ representing the ratio of diffusion coefficients reflects the fact that water diffuses more quickly than vegetation, while the advection term νV_x models the downhill flow of water on a (constantly) sloped terrain, whose slope is oriented in the x-direction, with the coefficient ν describing the grade of the slope. The primary differences between the model (5.1) and Klausmeier's original model [35] are the inclusion of the large diffusion term in the water (V) equation, and the additional factor $(1-\mu_2 U)$ in the nonlinearity in the U equation, representing the carrying capacity of soil.

Remark 5.1. We note that Klausmeier's original work [35] and many other studies [12, 23, 48] of the model (5.1) do not include the soil carrying capacity factor $(1-\mu_2 U)$ (i.e., the case $\mu_2 = 0$ representing infinite carrying capacity is considered). However, it is necessary to take $\mu_2 > 0$ here in order to apply the results of section 2.3. This is due to the fact that the fast layer problem (2.5) associated with (5.1) is no longer bistable in the degenerate case $\mu_2 = 0$, which in turn means Assumption 1 cannot be satisfied.

Remark 5.2. In [5], the parameter ν was assumed large, which reflects the comparatively fast timescale on which water V flows downhill (modeled via the advection term in the u equation) compared to the rate at which the vegetation U diffuses. It was shown in [5] in the absence of the diffusion term in the V equation, i.e., in the limit $\delta \to \infty$ that stable planar vegetation fronts and stripes can form, aligned in the direction transverse to the slope of the terrain. Ecologically, one expects, however, that water does diffuse due to soil-water transport, and at a rate faster than that of vegetation [29], so that, in fact, one should include a large diffusion term in the V equation, as in (5.1).

The system (5.1) was analyzed in the absence of advection, i.e., $\nu = 0$ in [14, section 4.1], where it was shown that bistable interfaces are *always* unstable to long wavelength perturbations. Using the results of sections 3–4, we show below that this same instability is present throughout the weak advection regime, but that the presence of sufficiently large ($\nu \gg 1$) advection can stabilize the fronts to long wavelength perturbations.

In (5.1), the set $\mathcal{S} = \{F(U, V; \boldsymbol{\mu}) = 0\}$ is comprised of three branches

$$
U = 0, \qquad U = U_F^{\pm}(V) := \frac{1 \pm \sqrt{1 - \frac{4\mu_1\mu_2}{V}}}{2\mu_2},
\tag{5.3}
$$

where the latter two branches are defined in the region $V \geq 4\mu_1\mu_2$. To find steady states, we solve

$$F(U,V;\boldsymbol{\mu}) = G(U,V;\boldsymbol{\mu}) = 0, \tag{5.4}$$

and deduce that (5.1) admits a stable steady state $(U^-,V^-) := (0,\mu_3)$ corresponding to zero vegetation (the "desert" state). When

$$\frac{\mu_3}{\mu_1} > 2\left(\mu_2 + \sqrt{1+\mu_2^2}\right) \tag{5.5}$$

there are two additional steady states $(U,V) = (U_{1,2},V_{1,2})$ representing uniform vegetation where

$$U_{1,2} = \frac{\mu_3 \pm \sqrt{\mu_3^2 - 4\mu_1(\mu_1+\mu_2\mu_3)}}{2(\mu_1+\mu_2\mu_3)}, \qquad V_{1,2} = \mu_3 - \frac{\mu_1 U_{1,2}}{1-\mu_2 U_{1,2}}.$$

Furthermore, when

$$\frac{\mu_3}{\mu_1} > 4\mu_2 + \frac{1}{\mu_2} \tag{5.6}$$

the state $(U^+,V^+) := (U_2,V_2)$ is PDE stable, i.e., the condition 1(i) is satisfied, while the remaining steady state (U_1,V_1) is always unstable [5]. Within the set $\mathcal{S}$, the branches

$$\mathcal{S}^- := \left\{U = f^-(V) \equiv 0\right\}, \qquad \mathcal{S}^+ := \left\{U = f^+(V) \equiv U_F^+(V),\right\} \tag{5.7}$$

contain the steady states of interest: the state (U^-,V^-) always lies on the branch $\mathcal{S}^-$, and when (5.6) is satisfied, the state (U^+,V^+) resides on $\mathcal{S}^+$; see Figure 5. When considering bistable traveling fronts, we are therefore interested in fronts between the steady states (U^-,V^-) and (U^+,V^+) in the parameter regime (5.6) which traverse a singular heteroclinic orbit of the fast layer equation

$$0 = U_{\xi\xi} + cU_\xi - \mu_1 U + U^2 V(1-\mu_2 U) \tag{5.8}$$

between the branches $\mathcal{S}^-$ and $\mathcal{S}^+$. We note that the cubic nonlinearity allows for the explicit construction of heteroclinic orbits in (5.8) between $\mathcal{S}^-$ and $\mathcal{S}^+$ for each $v_* > 4\mu_1\mu_2$; see, e.g., [5, section 2] or [14, section 4.1].

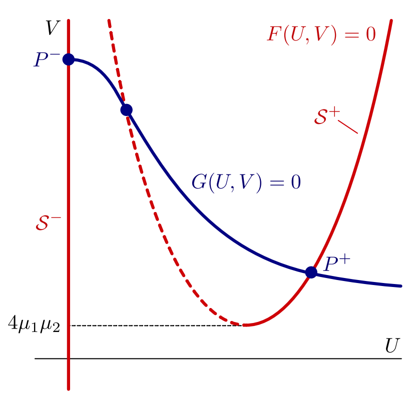

FIG. 5. *Sketch of the nullclines of* (5.2) *in the case* (5.6)*, depicting the branches* $\mathcal{S}^\pm$ *and equilibria* $P^\pm$.

Using geometric singular perturbation techniques as in [5], and separately considering the scalings in sections 3-4, it is possible to rigorous construct bistable traveling fronts between $(U^{\pm}, V^{\pm})$ in (5.1) for $0 < \delta \ll 1$. Since we are primarily interested in the effect of advection on the stability of such interfaces, we do not carry out a detailed existence analysis here, but point to other works which rigorously construct traveling fronts and other traveling or stationary waves in various parameter regimes in the same equation (5.2): in particular, the condition (Assumption 5) necessary for existence in the strong advection regime is verified in [5], while in the weak advection and intermediate regimes, Assumption 4 can be verified using similar techniques as in [10]. Therefore, in the remainder we assume the existence of a family of traveling fronts $\phi_{\mathrm{h}}(\xi;\nu,\delta) = (u_{\mathrm{h}}, v_{\mathrm{h}})(\xi;\nu,\delta)$ for $0 \le \nu < \infty$ and sufficiently small $\delta \ll 1$.

Figure 6 depicts the results of numerically continuing the coefficient $\lambda_{\mathrm{c},2}$ in AUTO using the formula (2.14) along such a family of fronts for fixed $\delta = 0.001$ and a wide range of ν values. We now examine the behavior of the coefficient $\lambda_{\mathrm{c},2}$ in the context of the asymptotic results of sections 3–4. We evaluate

$$\begin{aligned} F_v(u_*(\xi), v_*) &= u_*(\xi)^2\left(1 - \frac{u_*(\xi)}{\mu_2}\right) > 0,\\ G(u_*^+, v_*) - G(u_*^-, v_*) &= -v_*(u_*^+)^2 < 0 \end{aligned}$$

from which we immediately deduce from (2.16) that $F_* > 0$ and $G_* < 0$. In particular, in the weak advection regime, this determines the sign of $\lambda_{\mathrm{c},2}$ to be positive, and thus bistable planar fronts are always unstable to long wavelength perturbations in this regime. This agrees with the results of [14, section 4.1] in which the same equation was analyzed in the absence of advection ($\nu = 0$). In the strong advection regime, based on the results of section 4, we find that the coefficient $\lambda_{\mathrm{c},2}$ eventually changes sign as ν increases, so that suitably large advection therefore stabilizes the fronts to long wavelength perturbations. Comparing with Figure 6, which plots the coefficient $\lambda_{\mathrm{c},2}$ as a function of ν, and we observe that its sign indeed changes upon increasing ν at $\nu \approx 1472$. We recall that the asymptotic results of section 3.2.2 predict the change of sign to occur when $\nu \sim \delta^{-4/3}$. In Figure 7, we plot the results of continuing the equation $\lambda_{\mathrm{c},2} = 0$ in the parameters ν, δ. A log-log plot of ν versus δ demonstrates good agreement with the predicted $-4/3$ exponent. For larger values of ν, we see in Figure 6 that $\lambda_{\mathrm{c},2}$ remains negative and approaches -1 as $\nu \to \infty$,

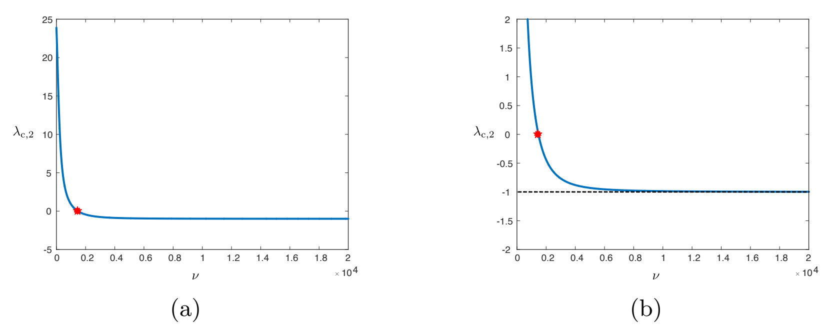

FIG. 6. (a) *Shown is a continuation branch of traveling front solutions of* (5.1) *over a range of* $\nu \in [0, 2\cdot 10^4]$ *for fixed* $\delta = 0.001$ *and* $\boldsymbol{\mu} = (0.1, 0.1, 2.0)$*, computed in AUTO-*07*p. The coefficient* $\lambda_{\mathrm{c},2}$ *is plotted versus* ν*. We observe that* $\lambda_{\mathrm{c},2}$ *changes sign as* ν *increases at* $\nu \approx 1472$*, denoted by the red star.* (b) *Vertical zoom of the same plot as in* (a)*, showing the horizontal asymptote* $\lambda_{\mathrm{c},2} = -1$*. (Figure in color online.)*

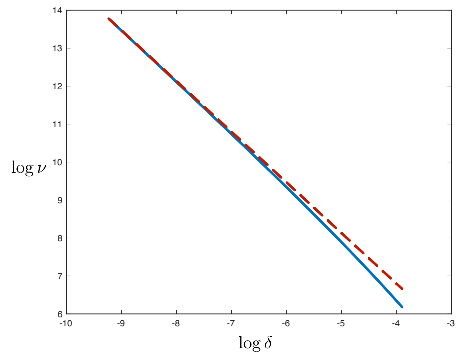

FIG. 7. *Results obtained by numerical continuation of the equation* $\lambda_{c,2} = 0$ *in AUTO-07p for values of* $\delta \in [0.0001, 0.02]$ *and system parameters* $\boldsymbol{\mu} = (0.1, 0.1, 2.0)$*: a log-log plot of* ν *versus* δ *(blue) is shown alongside a line of slope* $-4/3$ *(dashed red). (Figure in color online.)*

which further agrees with the asymptotic predictions in the strong advection regime in section 4.2.

6. Discussion. In this work, we examined the effect of advection on the stability of planar fronts in two spatial dimensions, motivated by observations of planar interfaces between desert and vegetated states in water limited ecosystems. In particular, we demonstrated a stabilizing mechanism of advection on a critical eigenvalue associated with long wavelength perturbations. In the context of application to dryland ecosystem models, this matches the common observation that interfaces between vegetation and bare soil present in vegetation patterns tend to align perpendicular to sloped terrain, on sufficiently steep slopes. The stability criteria posed in section 2.3 are formulated for general systems, which allows for straightforward application of the results to a wide class of reaction-diffusion-advection models, under modest assumptions. We discuss some of the implications and limitations of the assumptions and results below, as well as some open problems.

While the results of section 2.3 apply to a large class of models, we note that Assumption 1 limits the results to *bistable* traveling fronts. In particular, the results do not apply to the case of an invasion front into an unstable background state. The challenge is that one cannot as easily isolate instabilities associated with the *interface* of the front, due to the instability of the background state; in particular, one can no longer infer stability properties of the front in two spatial dimensions by simply expanding the marginal translation eigenvalue associated with 1D stability as in the current work. Typically such invasion fronts arise for an open range of wave speeds, with the selected wave speed resulting in either a pushed or pulled front, depending on whether the associated marginally stable spectrum is point or essential spectrum [2]. The subtle nature of these fronts makes even 1D stability a challenging problem, which has recently been analyzed for general multicomponent reaction diffusion systems in [1].

We emphasize that the results presented here concern the stability of single *straight* interfaces, in which a 1D front is trivially extended in the direction transverse to propagation to form a planar interface, which is a rather strong limitation, when considering the variety of patterns that can be observed in real dryland ecosystems and associated models. In particular, the model (5.1) and its variants support a wide variety of complex planar patterns, such as labyrinths, regular spot and gap patterns, and localized arc or crescent solutions [10, 27, 32, 49, 55]. In specific regimes, the existence and 2D spectral stability of more complex structures in (5.1) have been investigated using similar techniques. For instance, in the large advection limit, studies such as [5, 47] have considered other planar traveling waves such as stripes and curved interfaces, and in the case of flat terrain (no advection), an existence and stability analysis of radially symmetric structures has been carried out in [10], in which the stability of the resulting circular interface was linked to the stability of a straight planar interface in (5.1) in the limit of large radius. The analysis of (1.1) for all values of the advection coefficient ν in the current work can be seen as an initial step towards specifically analyzing the role played by advection in the dynamics of planar interfaces in systems such as (5.1).

These initial findings suggest numerous avenues for investigating the interplay of advection and diffusion on stability problems for traveling waves beyond one spatial dimension. In particular, for systems such as (5.1), where the quantities F_*, G_* are such that $\lambda_{\mathrm{c},2} > 0$ when $\nu = 0$, we expect an exchange of stability upon increasing the advection ν, occurring at a critical scaling $\nu \sim \delta^{-4/3}$. However, the coefficient $\lambda_{\mathrm{c},2}$ gives only a spectral stability criterion, so a natural question concerns the manifestation of the instability in the full nonlinear dynamics of (1.1) which manifests as ν decreases through this critical value. Such interfacial instabilities (in the absence of advection) have been examined in other ecosystems models (see, e.g., [14, 25]), where the emergence of finger-like protrusions and cusps have been observed. Figures 8–9 show the result of direct numerical simulations in the model (5.2). We observe the appearance of bounded cusp-like instabilities appearing in the planar interface for values of ν near (but below) the critical scaling $\nu \sim \delta^{-4/3}$. While this cusping behavior also appears for smaller values of ν in some parameter regimes, in other regimes (see Figure 9) we observe the development of finger-like instabilities in the interface, suggesting that this could perhaps be a more severe manifestation of this interfacial instability. An unfolding of the stability boundary at the critical scaling $\nu \sim \delta^{-4/3}$, and an analytical treatment of the emergent nonlinear behavior is the subject of ongoing work.

Lastly, while the results presented here are of a formal asymptotic nature, we emphasize that they could be obtained rigorously using geometric singular perturbation

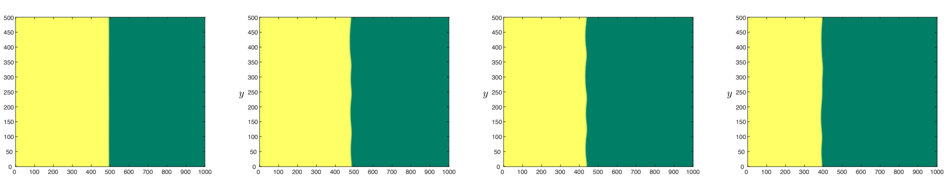

FIG. 8. *Shown are the results of direct numerical simulation in* (5.2) *for* $\delta = 0.01$, $\boldsymbol{\mu} = (0.1, 0.1, 2.0)$, *and* $\nu = 1200$, *which is below the critical stability boundary at which* $\lambda_{\mathrm{c},2}$ *changes sign (estimated at* $\nu \approx 1472$*). The simulation was initialized with a perturbation of the corresponding traveling front* $\phi_{\mathrm{h}}(\xi;\nu,\delta)$ *(obtained by numerically solving the traveling wave equation* (2.2)*) extended trivially in the y-direction. The PDE* (5.2) *was solved in a co-moving frame; finite differences were used for spatial discretization and MATLAB's ode*15*s routine was used for time integration. The panels depict the U-profile at times* $t = \{10000, 30000, 60000, 90000\}$ *(from left to right). Yellow indicates the bare soil state, while green indicates a vegetated state. We observe that after long simulation times, the front interface exhibits bounded cusping behavior, reminiscent of Kuramoto–Sivashinsky dynamics associated to a sideband instability* [21, 31]. *While the same cusping behavior appeared for these parameters at smaller values of* ν, *finger-like protrusions may appear for smaller values of* ν *in other parameter regimes; see Figure* 9.

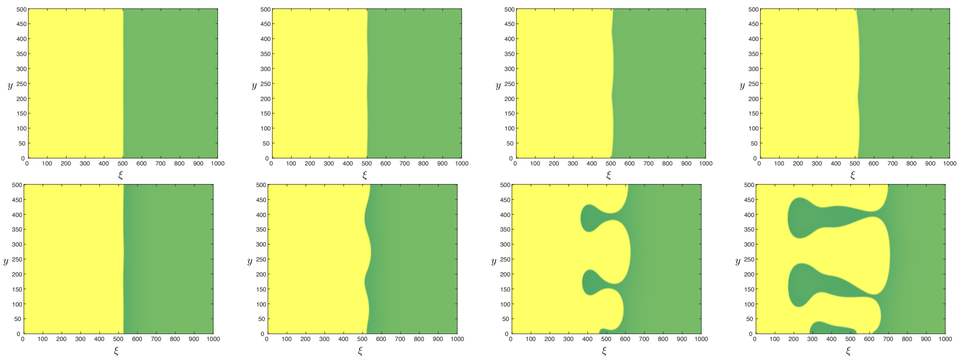

FIG. 9. *Shown are the results of direct numerical simulations in* (5.2) *for* $\delta = 0.01$ *and* $\boldsymbol{\mu} = (1.2, 1.0, 6.2)$*, performed similarly as those in Figure* 8*. The top row depicts the* U*-profile of the solution in the case* $\nu = 500$ *at times* $t = \{5000, 10000, 15000, 20000\}$*, while the bottom row depicts the solution in the case* $\nu = 50$ *at times* $t = \{2000, 3000, 4000, 5000\}$*. The critical stability boundary at which* $\lambda_{c,2}$ *changes sign was estimated at* $\nu \approx 819$ *for these parameter values. In the case* $\nu = 500$ *(top row) closer to the stability boundary, the same cusping behavior is observed as in Figure* 8*, while in the case* $\nu = 50$ *(bottom row) finger-like protrusions emerge on a comparatively shorter timescale.*

techniques. In particular, in the strong advection regime $\nu \geq \mathcal{O}(\delta^{-2})$ we expect it is possible to show rigorously that the fronts described here (as well as multi-front stripe and periodic patterned solutions) are stable in two spatial dimensions by analyzing (2.6) for all values of $\ell \in \mathbb{R}$ using a nearly identical approach as in [5, section 5], via exponential dichotomies and the Lin–Sandstede method [11, 38, 46]. A rigorous treatment of the stability of such structures is the subject of future work.

Appendix A. Stability of steady states. We briefly derive the conditions (2.4) of Assumption 1. Linearizing about the steady states $(U^\pm, V^\pm)$ of (1.1) and setting $(U,V)(x,y,t) = (U^\pm, V^\pm) + e^{\lambda t + ikx + i\ell y}(\bar{U}, \bar{V})$, we obtain the eigenvalue problem

$$\lambda \begin{pmatrix} \bar{U} \\ \bar{V} \end{pmatrix} = \begin{pmatrix} -(k^2+\ell^2) + F_u^\pm & F_v^\pm \\ G_u^\pm & -\dfrac{1}{\delta^2}(k^2+\ell^2) + i\nu k + G_v^\pm \end{pmatrix} \begin{pmatrix} \bar{U} \\ \bar{V} \end{pmatrix}. \tag{A.1}$$

The steady states $(U^\pm, V^\pm)$ are stable provided $\operatorname{Re}\lambda(k,\ell) < 0$ for any eigenvalue $\lambda(k,\ell)$ of (A.1), or equivalently, any $\lambda(k,\ell)$ satisfying

$$\lambda^2 + (p_1 + iq_1)\lambda + (p_2 + iq_2) = 0, \tag{A.2}$$

where

$$\begin{aligned} p_1 &= \left(1 + \frac{1}{\delta^2}\right)(k^2+\ell^2) - F_u^\pm - G_v^\pm, \\ q_1 &= -\nu k, \\ p_2 &= F_u^\pm G_v^\pm - F_v^\pm G_u^\pm - \left(\frac{F_u^\pm}{\delta^2} + G_v^\pm\right)(k^2+\ell^2) + \frac{1}{\delta^2}(k^2+\ell^2)^2, \\ q_2 &= -\nu k(k^2+\ell^2) + \nu k F_u^\pm. \end{aligned}$$

The corresponding roots of this quadratic have strictly negative real part if and only if (see, e.g., [26])

$$p_1 > 0, \tag{A.3}$$

$$p_1^2 p_2 + p_1 q_1 q_2 - q_2^2 > 0 \tag{A.4}$$

are satisfied for all $k, \ell \in \mathbb{R}$. The condition (A.3) implies that

$$F_u^{\pm} + G_v^{\pm} < 0 \tag{A.5}$$

while (A.4) implies (consider, e.g., $k = \ell = 0$)

$$F_u^{\pm} G_v^{\pm} - F_v^{\pm} G_u^{\pm} > 0. \tag{A.6}$$

Considering (A.4) for $k = 0$ and $\ell = \mathcal{O}(\delta)$ implies that $F_u^{\pm} < 0$, while setting $\ell = 0$, $k \ll 1$, and ν sufficiently large implies that $G_v^{\pm} < 0$ as well.

REFERENCES

[1] M. Avery, *Front selection in reaction–diffusion systems via diffusive normal forms*, Arch. Ration. Mech. Anal., 248 (2024), 16.

[2] M. Avery, M. Holzer, and A. Scheel, *Pushed and Pulled Fronts in a Logistic Keller-Segel Model with Chemorepulsion*, preprint, https://arxiv.org/abs/2308.01754, 2023.

[3] S. Banerjee, M. Baudena, P. Carter, R. Bastiaansen, A. Doelman, and M. Rietkerk, *Rethinking Tipping Points in Spatial Ecosystems*, preprint, https://arxiv.org/abs/2306.13571, 2023.

[4] N. Barbier, P. Couteron, and V. Deblauwe, *Case study of self-organized vegetation patterning in dryland regions of central Africa*, in Patterns of Land Degradation in Drylands, Springer, 2014, pp. 347–356.

[5] R. Bastiaansen, P. Carter, and A. Doelman, *Stable planar vegetation stripe patterns on sloped terrain in dryland ecosystems*, Nonlinearity, 32 (2019), pp. 2759–2814.

[6] R. Bastiaansen, H. A. Dijkstra, and A. S. von der Heydt, *Fragmented tipping in a spatially heterogeneous world*, Environ. Res. Lett., 17 (2022), 045006.

[7] J. J. Bennett and J. A. Sherratt, *Large scale patterns in mussel beds: Stripes or spots?*, J. Math. Biol., 78 (2019), pp. 815–835.

[8] F. Borgogno, P. D'Odorico, F. Laio, and L. Ridolfi, *Mathematical models of vegetation pattern formation in ecohydrology*, Rev. Geophys., 47 (2009), RG1005.

[9] A. I. Borthagaray, M. A. Fuentes, and P. A. Marquet, *Vegetation pattern formation in a fog-dependent ecosystem*, J. Theoret. Biol., 265 (2010), pp. 18–26.

[10] E. Byrnes, P. Carter, A. Doelman, and L. Liu, *Large amplitude radially symmetric spots and gaps in a dryland ecosystem model*, J. Nonlinear Sci., 33 (2023), 107.

[11] P. Carter, B. de Rijk, and B. Sandstede, *Stability of traveling pulses with oscillatory tails in the FitzHugh–Nagumo system*, J. Nonlinear Sci., 26 (2016), pp. 1369–1444.

[12] P. Carter and A. Doelman, *Traveling stripes in the Klausmeier model of vegetation pattern formation*, SIAM J. Appl. Math., 78 (2018), pp. 3213–3237, https://doi.org/10.1137/18M1196996.

[13] P. Carter, A. Doelman, A. Iuorio, and F. Veerman, *Travelling Pulses on Three Spatial Scales in a Klausmeier-Type Vegetation-Autotoxicity Model*, preprint, https://arxiv.org/abs/2312.12277, 2023.

[14] P. Carter, A. Doelman, K. Lilly, E. Obermayer, and S. Rao, *Criteria for the (in)stability of planar interfaces in singularly perturbed* 2*-component reaction–diffusion equations*, Phys. D, 444 (2023), 133596.

[15] X. Chen, R. Hambrock, and Y. Lou, *Evolution of conditional dispersal: A reaction–diffusion–advection model*, J. Math. Biol., 57 (2008), pp. 361–386.

[16] V. Deblauwe, P. Couteron, J. Bogaert, and N. Barbier, *Determinants and dynamics of banded vegetation pattern migration in arid climates*, Ecol. Monogr., 82 (2012), pp. 3–21.

[17] V. Deblauwe, P. Couteron, O. Lejeune, J. Bogaert, and N. Barbier, *Environmental modulation of self-organized periodic vegetation patterns in Sudan*, Ecography, 34 (2011), pp. 990–1001.

[18] M. Desroches, J. Guckenheimer, B. Krauskopf, C. Kuehn, H. M. Osinga, and M. Wechselberger, *Mixed-mode oscillations with multiple time scales*, SIAM Rev., 54 (2012), pp. 211–288, https://doi.org/10.1137/100791233.

[19] A. Doelman, *Slow localized patterns in singularly perturbed two-component reaction–diffusion equations*, Nonlinearity, 35 (2022), pp. 3487–3559.

[20] A. Doelman, D. Iron, and Y. Nishiura, *Destabilization of fronts in a class of bistable systems*, SIAM J. Math. Anal., 35 (2004), pp. 1420–1450, https://doi.org/10.1137/S0036141002419242.

[21] A. Doelman, B. Sandstede, A. Scheel, and G. Schneider, *The Dynamics of Modulated Wave Trains*, Mem. Amer. Math. Soc. 934, AMS, Providence, RI, 2009.

[22] L. Eigentler, *Species coexistence in resource-limited patterned ecosystems is facilitated by the interplay of spatial self-organisation and intraspecific competition*, Oikos, 130 (2021), pp. 609–623.

[23] L. Eigentler and J. A. Sherratt, *Analysis of a model for banded vegetation patterns in semi-arid environments with nonlocal dispersal*, J. Math. Biol., 77 (2018), pp. 739–763.

[24] N. Fenichel, *Geometric singular perturbation theory for ordinary differential equations*, J. Differential Equations, 31 (1979), pp. 53–98.

[25] C. Fernandez-Oto, O. Tzuk, and E. Meron, *Front instabilities can reverse desertification*, Phys. Rev. Lett., 122 (2019), 048101.

[26] E. Frank, *On the zeros of polynomials with complex coefficients*, Bull. Amer. Math. Soc., 52 (1946), pp. 144–157.

[27] P. Gandhi, L. Werner, S. Iams, K. Gowda, and M. Silber, *A topographic mechanism for arcing of dryland vegetation bands*, J. Roy. Soc. Interface, 15 (2018), 20180508, https://doi.org/10.1098/rsif.2018.0508.

[28] J. Ge, K. I. Kim, Z. Lin, and H. Zhu, *A sis reaction–diffusion–advection model in a low-risk and high-risk domain*, J. Differential Equations, 259 (2015), pp. 5486–5509.

[29] E. Gilad, J. von Hardenberg, A. Provenzale, M. Shachak, and E. Meron, *Ecosystem engineers: From pattern formation to habitat creation*, Phys. Rev. Lett., 93 (2004), 098105.

[30] U. Helldén, *Desertification monitoring: Is the desert encroaching?*, Desertification Control Bull., 17 (1988), pp. 8–12.

[31] J. M. Hyman and B. Nicolaenko, *The Kuramoto-Sivashinsky equation: A bridge between PDE's and dynamical systems*, Phys. D, 18 (1986), pp. 113–126.

[32] A. Iuorio, N. Salvatori, G. Toraldo, and F. Giannino, *Analysis and numerical simulations of travelling waves due to plant–soil negative feedback*, European J. Appl. Math., (2023), pp. 1–12.

[33] P. Kaklamanos, N. Popović, and K. U. Kristiansen, *Geometric singular perturbation analysis of the multiple-timescale Hodgkin–Huxley equations*, SIAM J. Appl. Dyn. Syst., 22 (2023), pp. 1552–1589, https://doi.org/10.1137/22M1477477.

[34] T. Kapitula and K. Promislow, *Spectral and Dynamical Stability of Nonlinear Waves*, Appl. Math. Sci. 185, Springer, New York, 2013.

[35] C. A. Klausmeier, *Regular and irregular patterns in semiarid vegetation*, Science, 284 (1999), pp. 1826–1828.

[36] T. Kolokolnikov, M. Ward, J. Tzou, and J. Wei, *Stabilizing a homoclinic stripe*, Philos. Trans. Roy. Soc. A, 376 (2018), 20180110.

[37] C. Kuehn, N. Berglund, C. Bick, M. Engel, T. Hurth, A. Iuorio, and C. Soresina, *A general view on double limits in differential equations*, Phys. D, 431 (2022), 133105.

[38] X.-B. Lin, *Using Melnikov's method to solve Silnikov's problems*, Proc. Roy. Soc. Edinburgh Sect. A, 116 (1990), pp. 295–325.

[39] R. N. Lipcius, D. G. Matthews, L. Shaw, J. Shi, and S. Zaytseva, *Facilitation between Ecosystem Engineers, Salt Marsh Grass and Mussels, Produces Pattern Formation on Salt Marsh Shorelines*, bioRxiv, 2021, https://doi.org/10.1101/2021.04.14.439864.

[40] J. Ludwig, B. Wilcox, D. Breshears, D. Tongway, and A. Imeson, *Vegetation patches and runoff-erosion as interacting ecohydrological processes in semiarid landscapes*, Ecology, 86 (2005), pp. 288–297.

[41] H. Malchow, *Nonlinear plankton dynamics and pattern formation in an ecohydrodynamic model system*, J. Marine Syst., 7 (1996), pp. 193–202.

[42] E. Meron, *Pattern-formation approach to modelling spatially extended ecosystems*, Ecol. Model., 234 (2012), pp. 70–82.

[43] Y. Nishiura, M. Mimura, H. Ikeda, and H. Fujii, *Singular limit analysis of stability of traveling wave solutions in bistable reaction-diffusion systems*, SIAM J. Math. Anal., 21 (1990), pp. 85–122, https://doi.org/10.1137/0521006.

[44] M. Rietkerk and J. Van de Koppel, *Regular pattern formation in real ecosystems*, Trends Ecol. Evol., 23 (2008), pp. 169–175.

[45] A. B. Rovinsky and M. Menzinger, *Chemical instability induced by a differential flow*, Phys. Rev. Lett., 69 (1992), 1193.

[46] B. Sandstede, *Stability of multiple-pulse solutions*, Trans. Amer. Math. Soc., 350 (1998), pp. 429–472.

[47] L. Sewalt and A. Doelman, *Spatially periodic multipulse patterns in a generalized Klausmeier–Gray–Scott model*, SIAM J. Appl. Dyn. Syst., 16 (2017), pp. 1113–1163, https://doi.org/10.1137/16M1078756.

[48] J. A. Sherratt, *An analysis of vegetation stripe formation in semi-arid landscapes*, J. Math. Biol., 51 (2005), pp. 183–197.

[49] E. Siero, A. Doelman, M. Eppinga, J. D. Rademacher, M. Rietkerk, and K. Siteur, *Striped pattern selection by advective reaction-diffusion systems: Resilience of banded vegetation on slopes*, Chaos, 25 (2015), 036411.

[50] K. Siteur, E. Siero, M. B. Eppinga, J. D. Rademacher, A. Doelman, and M. Rietkerk, *Beyond Turing: The response of patterned ecosystems to environmental change*, Ecol. Complex., 20 (2014), pp. 81–96.

[51] M. Taniguchi, *Instability of planar traveling waves in bistable reaction-diffusion systems*, Discrete Contin. Dyn. Syst. Ser. B, 3 (2003), pp. 21–44.

[52] M. Taniguchi and Y. Nishiura, *Instability of planar interfaces in reaction-diffusion systems*, SIAM J. Math. Anal., 25 (1994), pp. 99–134, https://doi.org/10.1137/S0036141092233500.

[53] G. A. UN, *Transforming our World: The* 2030 *Agenda for Sustainable Development*, Technical report, A/RES/70/1, 2015.

[54] C. Valentin, J. d'Herbès, and J. Poesen, *Soil and water components of banded vegetation patterns*, Catena, 37 (1999), pp. 1–24.

[55] T. Wong and M. J. Ward, *Dynamics of patchy vegetation patterns in the two-dimensional generalized Klausmeier model*, Discrete Contin. Dyn. Syst. Ser. S, 15 (2022), pp. 2747–2793.

[56] Y. R. Zelnik, H. Uecker, U. Feudel, and E. Meron, *Desertification by front propagation?*, J. Theoret. Biol., 418 (2017), pp. 27–35.